Responses to Reviewers of acp-2015-382 “Controlled meteorological (CMET) free balloon profiling of the Arctic atmospheric boundary layer around Spitsbergen”

T.J. Roberts, M. Dütsch, L. R. Hole, P. Voss

We thank the two anonymous referees and GJ Steeneveld for their reviews and comments. These have greatly helped us revise the manuscript. We have refocused the manuscript scope following the comment of Anonymous Referee #3 to no longer include the WRF simulations that had some issues. Rather we compare the CMET measurements to the ERA-I reanalysis product and to a new high resolution (15 km) Arctic System Reanalysis. The main focus of the manuscript is the same: demonstrating the CMET balloons with in-flight repeated soundings as a new technology to probe the remote Arctic troposphere and boundary layer. The major science change we have made is about the model output used to compare to the CMET observations. The text has been updated accordingly. The structure is:

Title
Abstract
1 Introduction
2. Methods:
2.1 CMET balloon and payload description
2.2 Balloon Launches in Svalbard
2.3 Model reanalyses produces ERA-I and ASR
3. Results and Discussion
3.1 Meteorological conditions during the campaign
3.2 CMET profiles over sea-ice compared to ERA-I and ASR
3.3 CMET profiles in coastal area compared to ERA-I and ASR
3.4 CMET soundings in detail: decoupled flows and wind-field estimation
3.5 Discussion: ASR and ERA-I model reanalyses in comparison to CMET
4 Conclusions

Below we write our responses to the reviewer comments followed by track-changes illustration of all changes made to the manuscript. Given the improvements made, several sections of text have been re-written to reflect the revised focus. Specific improvements to the figures include: comparison between 4-D interpolated ASR & ERA-I model data and CMET observations, which is more instructive than the simple transects presented for WRF previously. Spatial maps of surface temperature and humidity over the course of the day (JD 131) are also presented to enable visual distinction between diurnal effects and advection, presented as part of the discussion. The wind-roses have been corrected for an error in the original figures (that the software does not automatically calculate from due North, as might be expected). The Ny-Alesund time-series is now presented using publically available minute data rather than 6-hrly averaged data presented previously. Figures have also been improved for general clarity, and size of fonts.

Anonymous Referee #3

This paper presents the use of a new balloon technology to obtain numerous vertical soundings during a flight, an extremely useful tool for improving knowledge of weather with links to to climate in the Arctic region. Then, the balloon data is compared with the regional weather model WRF run during the same period. The strength of this paper is the measurements, there are some concerns about the WRF modeling that make it difficult to draw conclusions about the model performance as already pointed out by the short comment by GJ Steeneveld. This is a really interesting and exciting measurement technique and upon addressing the major and minor comments, the paper should be accepted as it's well within the scope of ACP.

We thank the reviewer for their detailed reading of the manuscript and useful comments. We appreciate the concerns expressed on the modelling aspect of the manuscript and have undertaken revisions to improve on these issues as described below.

Major comments:

- Recently a large problem in the surface skin temperature for the Noah Land Surface Model (LSM) over snow/ice was discovered and corrected in the most recent version of WRF (see comments for most recent WRF release 3.7.1 found online http://www2.mmm.ucar.edu/wrf/users/wrfv3.7/updates-3.7.1.html). This issue combined with the issue pointed for the YSU boundary layer scheme (noted in the short comment by GJ Steeneveld) make it clear that the model should be re-run and compared with the CMET data using the most recent WRF version, where these bugs have been corrected. In addition, the authors note they did not use fractional sea ice, which is currently commonly used for runs in the Arctic region. Finally, the authors didn't use any type of restart or nudging for the outer domain, which is also commonly used to ensure large scale meteorological features don't diverge from ECMWF.

- Rather than fixing all of these issues with the WRF run, it would be easier (and possibly even more convincing) for the authors to focus on the measurements and compare the CMET results with the meteorological forecast provided by ECMWF directly (currently these are used as the boundary conditions and initial conditions for their WRF run). Then, the authors can focus on the measurements and how they compare with ECMWF, the meteorological features that determine the balloon movement, and where the measurements and ECMWF do not agree, pointing to where the model can be improved in the future.

We thank the reviewer for this advice which we have taken. We compare the CMET data to ECMWF ERA-I reanalysis model level data. However, this is quite coarse resolution (~80 km, even if we downloaded it at higher resolution – this is simply interpolated from the parent model data). We therefore also chose to compare to a very new reanalysis product (Arctic System Reanalysis: ASR) at high horizontal (15 km) and vertical resolution (about double the number of model levels in lower troposphere compared to ERA-I). The revised manuscript focus is on presenting the CMET technology for automated soundings into the Arctic BL and comparing the CMET observations from two flights to 4-D interpolated model data from two reanalyses. The revised manuscript first discusses the meteorological conditions of the study then compares the CMET observations with 4D interpolated model data for two flights that made automated/repeated soundings into the ABL. We discuss possible reasons for differences in the model outputs and also present detailed analysis of CMET flight to derive wind-fields.

We appreciate the concerns expressed with the original WRF modelling that is no longer include in the revised manuscript, instead we compare CMET to ERA-I and ASR outputs. For a future follow-up WRF study we will follow these recommendations. Regarding this study: we note that both ERA-I and ASR include fractional sea-ice (sea-ice description is most detailed in ASR). ASR uses Polar WRF 3.3.1 with MYNN boundary layer scheme (Bromwich et al., 2012), rather than YSU which was reported to have a bug. ASR includes nudging above 100 hPa. The use of data assimilation will also help to constrain the model.

Regarding the recently discovered bug in surface skin temperature for LSM over snow/ice: it is possible that this bug is also present in ASR. Nevertheless, our comparison of ASR to CMET flight 4 seems relatively good suggesting this bug was not critical in this case.

- The paper will be much stronger if the authors use the data to evaluate and improve WRF in a second paper mostly focused on modeling.

We agree and do consider a possible follow-up sensitivity study to compare CMET balloon flights to (polar) WFR using a range of boundary layer schemes/surface schemes.

Minor comments:

- The paper should be re-edited for clarity and wording

We have taken care to carefully revise the manuscript to make it clear. Given the major change in the modelling part there are sections of text that are completely reworded.

- I would suggest to move the meteorological overview from the supplement into the main text of the paper.

This has been moved to the start of the Results section.

- A few more details of how Figure 12 was generated and some more discussion of what this figure shows are needed.

We agree this figure was not well enough described in the original ms and have improved the description and included views of the 3D Figure from multiple angles. Please see response to reviewer 2 below.

Anonymous Referee #2

The paper compares model simulations carried out using a mesoscale meteorological model, with resolution down to 1 km, with observations from controlled meteorological balloons. This comparison bears on the polar atmospheric boundary layer, the balloons being laucnhed from Svalbard. The outcome demonstrates that the model fails to reproduce many characteristics of the observaed boundary layer. The balloon technology used is new and makes it possible to obtain numerous vertical soundings along a flight. This study is of interest both because it is a demonstration of the usefulness of these controlled meteorological balloons and because it shows the deificiencies of the mesoscale model at these high latitudes and in the presence of complex terrain and of fractional sea-ice. The paper is clearly written, the conclusions are well supported. I recommend publication after a minor revision.

We thank the reviewer for their detailed reading of the manuscript and useful comments.

Major points:

1. CMET balloons are a new technology and this paper is an important demonstration of the possibilities that these balloons offer for investigating the Boundary Layer. As they are new, it would be useful to give some more description of the balloons, their design and principle, and the implementation.At present, there are a few sentences at the top of p27543. We understand or imagine what the balloons may be. It would be best to give more details (principle, autonomy, timescales for a vertical sounding, ascent/descent rates, range of altitudes that can be sampled...). Of course, this is certainly described in Voss et al, 2013; but a few sentences in the present paper would make it more self-sufficient...

Detailed text has been added to Methods to describe the balloon design, principle of operation and the different sensors.

“Controlled Meteorological (CMET) balloons can fly for multiple days in the troposphere with altitude controlled via satellite link (Voss et al., 2012). Altitude control is achieved by the dual balloon design (high-pressure inner and low pressure outer balloon) between which helium is transferred by a miniature pump-valve system. Commands sent through an Iridium satellite link can set target altitude (typically 0–3500 m), control band (~50 – 500 m with the higher band using less power), vertical velocity (~0.5 - 1.5 m/s), termination countdown timer, and numerous other operational parameters. For this study, a new capacity was added to perform automated soundings between two specified pressure altitudes.

The 215-gram CMET payload (excluding balloon envelopes) includes the control electronics, GPS receiver, satellite modem, pump-valve system, lithium polymer battery, photovoltaic panel, aspirated T-RH sensor, and a vacuum-insulated pouch for the payload. The payload temperature is maintained within acceptable operating limits (typically +20 ˚C above ambient) even at altitudes of several kilometres in the Arctic.

An aviation-grade pressure sensor (Freescale MPXH6115A) coupled to a 16-bit analog-to-digital converter (Analog Devices AD7795) provides altitude information to the balloon's control algorithm every 10 seconds during flight. As part of data post-processing, this pressure-derived altitude is corrected for pressure offsets using the in-flight GPS altitude (Inventek ISM300X). GPS latitude and longitude provide the in-flight CMET coordinates and are also further analysed post-flight to determine wind speeds in eastward (U) and northward (V) directions.

Temperature is measured using a thermistor (General Electric MC65F103A) in a 10k-Ohm divider circuit coupled to the aforementioned analog-to-digital converter. A capacitance humidity sensor (G-TUCN.34 from UPSI, covering 2 to 98 % RH range over -40° C to + 85° C) generates a signal which is a function of the ambient relative humidity (RH) with respect to water. Relative humidity was converted to specific humidity (Q) for comparison to the ERA-I and ASR model outputs.

CMETs are easy to launch (requiring just 1-2 people with standard meteorological balloon skills: launches have been achieved under a wide range of surface winds to date) and are similar in size to a standard meteorological balloon. Further details of the CMET balloon, payload design and balloon flight engineering are described by Voss et al. (2012)."

2. The relative performances of the three ABL schemes used are not sufficiently described; the main conclusion insists that the three are fairly close together, and far from the observations, indicating that there is work yet to be done in understanding and modeling the polar ABL. Fine. Nonetheless, in the frame of the present study, were there some aspects which seemed better described with one scheme rather than the others?

We agree with the reviewer's comment that more information on the WRF schemes would be have been useful, as part of their discussion compared to CMET. Note that the revised ms no longer includes WRF, instead compares the CMET observations to two reanalyses (ASR and ERA-I). Care has been taken to describe these reanalyses products in Methods. In the conclusions we discuss that the higher vertical and horizontal resolution of ASR compared to ERA-I is probably important. We discuss that a follow-up WRF study might test e.g. different boundary layer schemes.

Minor points: p27540, line 11: useful to add preicison on finest resolution: 'nested grids down to 1 km'

This test no longer exists in the revised ms. We do describe the resolution of the two model reanalyses products in Methods. Our study indicates that resolution is likely an important aspect of model performance.

p27541, line 9: remove comma: 'processes, is' -> 'pocesses is' (commas around 'however' could also be removed)

Text updated.

p27542, lines 9-20: make a table perhaps (type of instrument, number of observations, publication..)? This sentence is not readable.

This paragraph on previous WRF studies no longer exists in the revised version. We agree that the original sentence was too long and a Table would be needed for long lists of studies.

p27543, line 2: commanded -> command

Text updated.

p27543, line 17: 'nunatak' will not be understood by many readers I expect; it may be justified to leave as is (and motivated readers will learn a new word...) or to change to something like "topographically induced convection", although less precise...

This text has been shortened in the new manuscript so nunatak is no longer mentioned.

p27546, line 22: 'Gulf Stream' -> North Atlantic Drift rather...

Corrected to North Atlantic Drift.

p27547, line 3: 'cumulus convection was neglected' -> 'the cumulus convection scheme was unused'

This text no longer exists given the revised ms scope.

p27548, line 2: become -> became line 3: 'given occurence of' -> 'due to the presence of'?

Corrected.

p27566, figure 5: fonts are too small

Care has been taken that all figures now have reasonable sized fonts.

p27568, figure 7: bottom right panel: for the direction, could the authors use or set up a color table that is periodic (ie the color for 360 should be the same as that for 0, eg by setting up the colormap twice, head to tail (there would be an inconvenient: a 180 degree ambiguity as each color would correspond to 2 angles) or by creating a periodic color table (eg blue to green to yellow to red to purple to blue)

This has been corrected to a periodic colorscheme for winddirection.

p27570, figure 9: color map should be the same for all three panels in each column

(see column 1, middel panel)

Care has been taken to ensure the revised figure panels now all have the same colormap.

p27570-1, figure 9, 11: it is somewhat misleading to show observations from the whole flight and a cross section at only one given time on the same plot. Perhaps the observations should be restricted to those within +/- 4 hours of the cross section

We agree this was not the best way to present and compare CMET and model data. We now perform full 4D interpolations (latitude, longitude, pressure, time) of the model data to the CMET balloon location in order to compare directly to the CMET observations. We present model output across a range of pressures (i.e. vertical transect at the CMET location) to aid interpretation of the observed and modelled along-flight meteorology.

p27573, figure 12 is difficult to read. This is perhaps an attempt to show too much information on one figure. The trajectories launched from a given height (black lines) seem fairly regular. Perhaps the authors could obtain a figure that is easier to read by showing only the balloon track and the final positions?

We agree that this is a complex figure and it wasn't described clearly enough. The wind-field was estimated from one CMET balloon flight, and the figure shows this flight, the starting point of the calculation, and wind-fields at regular altitude intervals that are calculated using wind-vectors from the balloon soundings. We now show the figure from three different angles to make it easier to understand. (we experimented with using different colors but found it did not help much). We also improve the text that describes the figure.

The new Figure caption reads: "Figure 12. Wind-field calculated from the CMET balloon flight 5. Air parcel trajectories are calculated over an eight hour period for each 50 m altitude layer according to the winds observed by the CMET soundings. The red line shows the actual balloon track, the black vertical line shows the initialization of the calculation, and the derived air parcel trajectories (wind field grid) are shown in gray. The blue line shows the final locations after eight hours."

The new text reads: "Wind-fields are estimated from the CMET balloon 5 flight path for an 8-hour period starting in the early morning of 11 May, Figure 12. As per previous figures, the CMET balloon movement during the soundings has been used to estimate wind-speed and direction. Here, wind-trajectories are derived from the observed winds at 50 m altitude intervals for each up or down profile. The trajectory vectors (of length proportional to the wind-speed × time elapsed between soundings) are placed end-to-end to estimate the wind-field, shown in Figure 15 (gray mesh) alongside the CMET flight (red). This approximate technique assumes horizontally uniform flow (in the vicinity of the balloon and computed trajectories). The lowermost layer exhibited greatest wind-speed thus has the longest (and least certain) trajectory, approximately double that of the balloon during the same period. The uppermost layer flows southwards before reversing direction, approximately returning to its initial position at 600 m altitude. The middle layer trajectory is quite similar to that of the overall CMET balloon flight…"

Comment by GJ Steeneveld

This is an interesting study that documents the WRF model performance against a new measurement technique for the challenging Arctic region.

Just two remarks:

-In the study you use the WRF 3.3.1 version. It is known that WRF versions older than the release 3.4.1 is suffering from a bug in the YSU scheme concerning the stable boundary layer. It appeared that the stability was not correctly activated. This results in too deep stable boundary layers, with low levels jets that are too much diluted (thick and low wind speeds). These have been documented in

Sterk, H. A. M., G. J. Steeneveld, and A. A. M. Holtslag (2013), The role of snowsurface coupling, radiation, and turbulent mixing in modeling a stable boundary layer over Arctic sea ice, J. Geophys. Res. Atmos., 118, 1199–1217, doi:10.1002/jgrd.50158

Sterk, H.A.M., G. J. Steeneveld, T. Vihma, P. S. Anderson, F. C. Bosveld, A. A. M. Holtslag, Clear-sky stable boundary layers with low winds over snow-covered surfaces. Part 1: WRF model evaluation, Quarterly Journal of the Royal Meteorological Society, 2015, 141, 691, 2165.

Xiao-Ming Hu, Petra M. Klein, Ming Xue, Evaluation of the updated YSU planetary boundary layer scheme within WRF for wind resource and air quality assessments, Journal of Geophysical Research: Atmospheres, 2013, 118, 18, 10,490

Although I believe the model biases that are shown also are the result of other aspects of the modelling effort, perhaps it is worth checking.

We thank GJ Steeneveld for highlighting these issues with WRF 3.3.1. In response to this and reviewer comments we changed our manuscript to now instead compare the CMET to ERA-I and ASR reanalysis data in this study. We will certainly take the comments about WRF into account for future follow-up studies using (polar) WRF.

-A second question is related to the land/snow-atmosphere coupling. The representation of the complex process of how to represent the heat and moisture transport from the subsurface and the land surface to the atmosphere is crucial. Do the model results remain the same in case another land-surface scheme is used?

We did not test different land-surface schemes with WRF, but we agree with the reviewer's comment that this can be important influence on the near-surface atmospheric conditions. This question should be considered in any follow-up sensitivity study using WRF. For this study our revised manuscript now compares CMET to ERA-I and ASR instead of WRF.

Controlled meteorological (CMET) free balloon profiling of the Arctic atmospheric boundary layer around Spitsbergen, compared to ~~a mesoscale model~~ERA-Interim and Arctic System Reanalyses

T. J. Roberts[1,2], M. Dütsch[3,4], L. R. Hole[3], P. B. Voss[5]

[1]{LPC2E/CNRS, 3A, Avenue de la Recherche Scientifique, 45071 Orléans, cedex 2, France}

[2]{Norwegian Polar Institute, Fram Centre, 9296 Tromsø, Norway}

[3]{Norwegian Meteorological Institute, Bergen, Norway}

[4]{ETH Zürich, Switzerland}

[5]{Smith College, Picker Engineering Program, Northampton MA, USA}

Correspondence to: T. J. Roberts (TjardaRoberts@gmail.com)

Abstract

Observations from CMET (Controlled Meteorological) balloons are analyzed ~~in combination with mesoscale model simulations~~ to provide insights into tropospheric meteorological conditions (temperature, humidity, ~~wind speed~~winds) around Svalbard, European High Arctic. Five Controlled Meteorological (CMET) balloons were launched from Ny-Ålesund in Svalbard (Spitsbergen Island) over 5-12 May 2011, and measured vertical atmospheric profiles ~~above Spitsbergen Island and~~ over coastal areas to both the east and west. One notable CMET flight achieved a suite of 18 continuous soundings that probed the Arctic marine boundary layer ~~over a period of more than 10 hours. The CMET profiles are compared to simulations using the Weather Research and Forecasting (WRF) model using nested grids and three different boundary layer schemes. Variability between the three model schemes was typically smaller than the discrepancies between the model runs and the observations. Over Spitsbergen, the CMET flights identified temperature inversions and low-level jets (LLJ) that were not captured by the model. Nevertheless, the model largely reproduced time-series~~

~~obtained from the Ny-Ålesund meteorological station, with exception of surface winds during the LLJ. Over sea-ice east of Svalbard the model underestimated potential temperature and overestimated wind-speed compared to the CMET observations. This is most likely due to the full sea-ice coverage assumed by the model, and consequent underestimation of ocean-atmosphere exchange in the presence of leads or fractional coverage. The suite of continuous CMET soundings over a sea-ice free region to the northwest of Svalbard are analysed spatially and temporally, and compared to the model. The observed along-flight daytime increase in relative humidity is interpreted in terms of the diurnal cycle, and in the context of marine and terrestrial air-mass influences. Analysis of the balloon trajectory during the CMET soundings identifies strong wind-shear, with a low-level channeled flow. The study highlights the challenges of modelling the Arctic atmosphere, especially in coastal zones with varying topography, sea-ice and surface conditions. In this context, CMET balloons provide a valuable technology for profiling the free atmosphere and boundary layer in remote regions where few other~~(ABL) over a period of more than 10 hours. Profiles from two CMET flights are compared to model output from ECMWF Era-Interim reanalysis (ERA-I), and to a high resolution (15 km) Arctic System Reanalysis (ASR) product. To the east of Svalbard over sea-ice the CMET observed a stable ABL profile with a temperature inversion that was reproduced by ASR but not captured by ERA-I. In a coastal ice-free region to the west of Svalbard the CMET observed a stable ABL with strong wind-shear. The CMET profiles document increases in ABL temperature and humidity that are broadly reproduced by both ASR and ERA-I. The ASR finds a more stably stratified ABL than observed but captured the wind-shear in contrast to ERA-I. Detailed analysis of the coastal CMET automated soundings identifies small-scale temperature and humidity variations with a low-level flow, and provides an estimate of local wind-fields. We demonstrate CMET balloons as a valuable approach to profile the free atmosphere and boundary layer in remote regions such as the Arctic where few other in-situ observations are available for model validation.

1 Introduction

~~The polar~~In remote regions ~~provide a challenge~~ such as the Arctic there exists very limited in-situ observational data to evaluate atmospheric ~~numerical~~ models. ~~Firstly, model parameterisations are often adapted to and validated against lower latitudes and might not necessarily be applicable to high latitude processes. Secondly, there exists limited~~ This study demonstrates CMET (Controlled Meteorological) balloons as a new approach for detailed ~~in-situ observational data for model initialization and validation in remote polar regions.~~ probing of the Arctic atmospheric boundary layer on local to regional scales, and compares the observations to model reanalysis outputs.

Accurate representation of polar meteorology and small-scale air-sea-ice interaction processes~~,~~ is~~, however,~~ essential for meteorological forecast models~~, whose comparison~~ and to ~~observations is particularly relevant for improving understanding of~~understand climate in the Arctic, a region undergoing rapid change (Vihma, 2014).~~A particular challenge is that the polar~~ The atmospheric boundary layer ~~(ABL)~~in the Arctic is usually strongly stable during winter~~,~~ and only weakly stable to neutral during summer (Persson et al., 2002). Strong temperature inversions can occur as warmer air masses from lower latitudes are advected over the cold polar air masses. This stability acts as a barrier to vertical atmospheric mixing and exchange, and can magnify ~~the effects of~~ flows over small~~-~~-scale topography~~,~~ such as ~~channeling,~~channelling and katabatic flows~~ and mountain waves, and can promote the formation of low-level jets. Further, in coastal areas,~~. The Barents Sea near Svalbard is especially implicated in Arctic climate (Smedsrud et al., 2013). To the east of Svalbard, the Barents Sea is typically partially covered by sea-ice during winter and spring, whilst sea-ice is typically absent in the Greenland Sea to the west of Svalbard. This is due to the northward flowing warm and saline Atlantic Warm Current (AWC) or 'North Atlantic Drift' that elevates temperatures along Svalbard's west coast, with a secondary branch that enters the Barents Sea. The warm saline AWC releases heat to the atmosphere as it cools to sink beneath the polar waters. The polar waters experience thermodynamic ~~ice~~ formation, growth and melt of sea-ice, and wind- and oceanic current driven advection of sea ice that can lead to highly variable surface conditions that ~~control~~affect air-sea exchange of heat and momentum, and ~~affect~~ the radiative balance e.g. through albedo. ~~Snow layers~~ Even at high sea-ice density, small patches of open water amongst very close (90%-100%) or close (80-90%) drift ice tend to promote sea-air exchange, enhancing both temperature and specific humidity at the surface (Andreas et al., 2002). Conversely, snow deposited upon sea-ice ~~provide a further~~ provides an insulating layer that ~~modifies heat exchange between the ocean and the overlying atmosphere. For example, for polar winter conditions at low atmospheric temperature (e.g. -40 ˚C), the surface temperature of open water areas is practically at the freezing point of water (-1.8 ˚C), while the surface temperature of thick snow covered sea ice is substantially lower, being close to the atmospheric temperature (e.g. -40 ˚C).~~reduces heat exchange. Hence, ~~the~~ heat and energy fluxes to the Arctic atmospheric boundary layer can vary by ~~up to two~~several orders of magnitude, depending on the surface state (Kilpeläinen et al., 2011).

~~Thus, significant uncertainties remain in modelling Arctic meteorological variables. For example, a comparison of eight different RCM (Regional Climate Model) simulations over the Western Arctic to European Center for Medium-Range Weather Forecast (ECMWF) analyses over Sept 1997- Sept 1998 found general agreement to the model ensemble mean but large across-model variability, particularly in the lowest model levels (Rinke et al., 2006). Direct comparisons of Arctic ABL meteorology observations to mesoscale model simulations using the regional Weather Research and Forecasting (WRF) model (in standard or 'polar' version) have also been performed. These include comparison to automatic weather stations (AWS) on the Greenland ice sheet in June 2001 and December 2002 (Hines and Bromwich, 2008); to drifting ice station SHEBA meteorological measurements over the Arctic Ocean in 1997-1998 (Bromwich et al., 2009); to tower observations and radio-sonde soundings in three Svalbard (Spistbergen) fjords in winter and spring 2008 (Kilpeläinen et al., 2011); to AWS stations along Kongsfjorden in Svalbard in spring 2010 (Livik, 2011); to meteorological mast measurements in Wahlenbergfjorden, Svalbard in May 2006 and April 2007 (Makiranta et al., 2011); to tethered balloon soundings and mast observations in Advent- and Kongsfjorden in Svalbard in March-April 2009 (Kilpeläinen et al., 2012), and to a remotely controlled model aircraft equipped with meteorological sensors (the small unmanned meteorological observer, SUMO) over Iceland and Advent valley in Svalbard (Mayer et al. (2012a;b). These studies collectively found that (Polar) WRF was able to partially reproduce the meteorological observations, typically only when operated at higher model resolution (e.g. 1 km). Sea-ice was found to be particularly important at high sea-air temperature differences, and occurrence of low-level jets were observed yet not always reproduced by the model. Such comparisons between model and observations are, however, limited by the spatial scale of the field observations, typically only a few km.~~

Model reanalyses provide temporally consistent representations of atmospheric and surface state, and are a valuable tool to understand Arctic processes and climate. A global model reanalysis product is ERA-Interim (ERA-I) from the European Centre for Medium-Range Weather Forecasts (ECMWF), Dee et al. (2011). At approximately 80 km resolution ERA-I has been widely used including for Arctic studies, e.g. Rinke et al. (2006). Recently, Arctic System Reanalysis (ASR) products have been developed at higher resolution (15 - 30 km) and specifically focused on high latitudes (Bromwich et al., 2016). There is an ongoing effort to validate and compare the ASR and ERA-I reanalyses datasets. The ASR (version 1: 30 km resolution) and ERA-I reanalyses exhibit comparable RMS errors for surface meteorology compared to Arctic-wide collated meteorological station data (December 2006-Novemeber 2007), Bromwich et al. (2016). Wind-speed biases were significantly smaller in the ASRv1. North of 60 °N, ASRv1 showed smaller precipitation biases than ERA-I except during summer. Moore et al. (2015) showed that the higher resolution ASRv1 is more able to fully resolve mesoscale features in the atmosphere, such as katabatic winds, to the south-east of Greenland, compared to ERA-I. Wesselen et al. (2014) compared ASRv1 and ERA-I reanalyses to surface and radiosonde meteorological data obtained during a 3 week ice-drift experiment in summer 2008, a period typically influenced by clouds. ERA-I was found to have a systematic warm bias in lowest troposphere, whilst ASRv1 had a systematic cold bias of similar magnitude. The ASR version 2 at 15 km resolution has recently been developed. Moore et al. (2016) demonstrate the added value of ASRv2 compared to ASRv1 in resolving topographically forced winds and capturing mesoscale spatial features around Greenland due to the higher resolution.

In this study we compare ASRv2 (at 15 km resolution) and ERA-I to in-situ CMET balloon observations in the Svalbard region during the 2011 Arctic spring. In this region in-situ measurements of the boundary layer and lower troposphere are limited. Meteorological stations provide continuous ground-based data and regular daily meteorological balloon profiles, but are sparsely located. In Svalbard, such datasets may be occasionally supplemented by tethered balloon or meteorological mast observations (e.g. Mäkiranta et al., 2011). Intensive field-campaigns probe more remote regions of the Arctic by aircraft (e.g. Vihma et al., 2005) or by drifting ice stations e.g. Rinke et al., (2006), Tjernström et al. (2012), but these can only be rarely undertaken due to cost. Remotely piloted aircraft systems (RPAS) also known as unmanned aerial vehicles (UAV) equipped with meteorological sensors provide an alternative cost-effective means to spatially probe the Arctic boundary layer around Svalbard at local scales, Mayer et al. (2012a;b). However, most UAVs are operated over timescales up to a few hours and over ranges typically limited to a few 10s of km. For low-altitude flights the range may be further limited if terrain blocks the signal.

To provide an in-situ meteorological ~~ABL~~ dataset ~~covering a~~ that samples the wider Svalbard Arctic region~~,~~ we deployed five Controlled ~~METteorological~~METeorological (CMET) balloons, launched in May 2011 from Ny-Ålesund ~~on~~in Svalbard. CMET balloons are capable of performing sustained flights within the troposphere at designated altitudes, and can ~~take~~make vertical soundings at any time during the balloon flight on ~~commanded~~command via satellite link (Voss et al., 2012). ~~The CMETs can also be configured for automated profiling of the atmospheric boundary layer during the flight, as we demonstrate in this study.~~ The nested dual balloon design ensures very little helium loss, enabling the balloons to make multi-day flights. This gives the opportunity to investigate areas far away from research bases, at greater spatial scales (many hundreds of kilometers from the launch point) than can be obtained by line-of-sight ~~unmanned aerial vehicle (~~RPAS/UAV~~)~~ approaches, radio-sondes or tethered balloons. ~~Previous CMET balloon applications include~~ The study builds upon previous uses of CMET balloons to probe regional scale meteorology including atmospheric trajectories (Riddle et al~~. (~~., 2006), air-flow downwind from a city pollution source (Voss et al. ~~(~~2010~~), Mentzoni (2011~~) and Antarctic meteorology on local to regional scales (Stenmark et al~~. (~~., 2014~~). Voss~~, Hole et al. ~~(2010) investigated~~2016). Here we demonstrate the ~~evolving vertical structure of~~ capability of CMET balloons to repeatedly make in-flight soundings down to low altitudes that reach into the ~~polluted Mexico City Area outflow by making repeated balloon profile measurements~~atmospheric boundary layer. We present multiple CMET flights of long duration (up to several days) in the Arctic including a CMET configured to make automated continuous profiling into the atmospheric boundary layer. These CMET in-situ profiles of temperature, humidity and ~~wind in the advecting outflow. Riddle et al. (2006)~~winds are compared to ERA-I and ~~Mentzoni (2011) used the CMET balloons as a tool to verify atmospheric trajectory models – namely FlexTra (Stohl et al., 1995) and FlexPart (Stohl et al., 1998) – in the United States and in the Arctic, respectively. Stenmark et al. (2014) combined data from CMETs, ground based and a small~~ASR model ~~airplane data with WRF simulations to highlight the role of nunatak-induced convection in Antarctica.~~ reanalyses.

~~Here we compare the soundings performed during the five Svalbard balloon flights of May 2011 to simulations made using the Weather Research and Forecasting (WRF) mesoscale model with three different boundary layer schemes, and thereby provide insights into key processes influencing meteorology of remote Arctic regions.~~

~~2 Methods~~

~~2.1 Observations~~

2. Methods

2.1 CMET balloon and payload description

Controlled Meteorological (CMET) balloons can fly for multiple days in the troposphere with altitude controlled via satellite link (Voss et al., 2012). Altitude control is achieved by the dual balloon design (high-pressure inner and low pressure outer balloon) between which helium is transferred by a miniature pump-valve system. Commands sent through an Iridium satellite link can set target altitude (typically 0–3500 m), control band (~50 – 500 m with the higher band using less power), vertical velocity (~0.5 - 1.5 m/s), termination countdown timer, and numerous other operational parameters. For this study, a new capacity was added to perform automated soundings between two specified pressure altitudes.

The 215-gram CMET payload (excluding balloon envelopes) includes the control electronics, GPS receiver, satellite modem, pump-valve system, lithium polymer battery, photovoltaic panel, aspirated T-RH sensor, and a vacuum-insulated pouch for the payload. The payload temperature is maintained within acceptable operating limits (typically +20 ˚C above ambient) even at altitudes of several kilometres in the Arctic.

An aviation-grade pressure sensor (Freescale MPXH6115A) coupled to a 16-bit analog-to-digital converter (Analog Devices AD7795) provides altitude information to the balloon's control algorithm every 10 seconds during flight. As part of data post-processing, this pressure-derived altitude is corrected for pressure offsets using the in-flight GPS altitude (Inventek ISM300X). GPS latitude and longitude provide the in-flight CMET coordinates and are also further analysed post-flight to determine wind speeds in eastward (U) and northward (V) directions.

Temperature is measured using a thermistor (General Electric MC65F103A) in a 10k-Ohm divider circuit coupled to the aforementioned analog-to-digital converter. A capacitance humidity sensor (G-TUCN.34 from UPSI, covering 2 to 98 % RH range over -40° C to + 85° C) generates a signal which is a function of the ambient relative humidity (RH) with respect to water. Relative humidity was converted to specific humidity (Q) for comparison to the ERA-I and ASR model outputs.

CMETs are easy to launch (requiring just 1-2 people with standard meteorological balloon skills: launches have been achieved under a wide range of surface winds to date) and are similar in size to a standard meteorological balloon. Further details of the CMET balloon, payload design and balloon flight engineering are described by Voss et al. (2012).

2.2 Balloon launches in Svalbard

Five CMET balloons were launched from the research station of the Alfred Wegener Institute and the Polar Institute Paul Emile Victor (AWIPEV) in Ny Ålesund, over the period 5 May to 12 May 2011~~. The CMET payload included meteorological sensors for temperature, relative humidity (RH) and pressure, as well as GPS and satellite modem for in-flight control. The CMET balloon design and control algorithms are described in detail by Voss et al. (2012). Figures 1a;b show the balloon flights of the May 2011 campaign as well as two meteorological sites providing additional ground-based data: the Ny Ålesund AWI-PEV station (from where the balloons were launched), and Verlegenhuken in North-East Spitzbergen.~~ (JD 125 to 132), Figure 1. Balloons 1 and 2 had short flights due to technical issues encountered at the start of the campaign~~, and included only one vertical sounding each.~~. Balloon 3 flew far north and was the longest duration flight in this campaign but did not perform any soundings after leaving the coastal area of ~~Spitzbergen, thus only the vertical sounding (ascent and descent) at the very beginning of the flight is used for this study~~Svalbard. Balloon 4 flew eastwards, but despite strong balloon performance needed to be terminated before encroaching Russian airspace. ~~In addition to its vertical sounding obtained shortly after launch it includes~~It performed two closely spaced (ascent and descent) soundings over sea-ice in the Barents Sea, east of Svalbard. Balloon 5 undertook a 24 hr duration flight that first exited Kongsfjorden, then flew northwards along the coast. It was placed into an automated sounding mode and ~~measured~~achieved a much longer series of 18 consecutive profiles of the ABL~~ in automatic sounding mode~~, before being raised to higher altitudes where winds advected it eastwards~~ (~~.~~Voss et al., 2012).~~ To the best of our knowledge, this was the first ~~automated sounding sequence~~demonstration of a set of extended controlled soundings made ~~by~~using a free balloon.

~~Temperature and humidity profiles were extracted from the CMET flights for model comparison as indicated in Figure 1a;b, in locations over Svalbard topography, over a sea-ice covered region east of Svalbard, and over a sea-ice free region west of Svalbard where continuous automated soundings were performed. The capacitance humidity sensor (G-TUCN.34 from UPSI, covering 2 to 98 % RH range over -40° C to + 85° C) generates a signal which is a function of the ambient relative humidity (RH) with respect to water. Humidity was therefore reported as RH over (supercooled liquid) water, which is standard procedure for atmospheric balloon-sonde measurements (even at sub-zero temperatures). Land- and/or sea-ice were, however, present for some of the campaign locations (although not during the automated soundings of flight 5 over ice-free ocean west of Svalbard). Where present, they could promote ice deposition, thus act to lower the water saturation vapour pressure. In such conditions, RH calculated over water underestimates the RH with respect to ice. Nevertheless, for the relatively warm ambient surface temperatures encountered over ice during the campaign (typically a few degrees negative ˚C or higher) such effects are modest. For consistency, RH over water is reported across the field-campaign and is similarly illustrated for the model output.~~

~~For comparison to two WRF nested model runs (see details below), the balloon profiles were interpolated to 50m height intervals and the measurement from paired ascent/descent soundings were averaged at each height. These ascent/descent profiles typically each required between 30 minutes and about one hour depending on the altitude change. These averaged ascent/descent profiles were compared to WRF model output at the longitude and latitude of the balloon location at the maximum of its ascent/descent cycle, averaged over a full hour centred on the middle of the balloon profile. A more detailed analysis was made of the meteorological evolution observed during consecutive automated soundings of flight 5, by comparing to WRF output at selected times along a transect line approximately following the CMET flight path, and geographically within the model layer corresponding to the average CMET flight altitude.~~

~~2.2 Numerical model implementation~~

~~Regional model simulations were performed using the Weather Research and Forecast (WRF) version 3.3.1. It is based on non-hydrostatic and fully compressible Euler equations that are integrated along terrain-following hydrostatic-pressure (sigma) coordinates, see Skamarock et al. (2008). The model was run for the simulation period from 3 May 2011 00:00 UTC to 12~~

~~May 2011 00:00 UTC allowing for a spin up time of 48 hours. An adaptive time-step was used (minimum 1 s) to avoid numerical instabilities. Three domains with a respective horizontal resolution of 9km, 3km and 1km were used, where the two inner domains both were two-way nested to their mother domain. The domain locations are shown in Figure 2. The outer domain was centered at 78.9◦ N, 16.5◦ E (78.9◦ N, 19.5◦ E for model run 2) and included 114 x 94 gridpoints covering the whole Svalbard archipelago and a large part of the surrounding Arctic ocean. The second domain included 175 x 184 (187 x 202) gridpoints for model run 1 (model run 2) and covered the whole Svalbard archipelago, whilst the innermost domain, which covered the area where the correspondent balloon profiles and timeseries were measured, had 232 x 190 (253 x 202) gridpoints for model run 1 (model run 2). All three domains had a high vertical resolution with 61 terrain-following sigma levels, where the model top was set to 50hPa. The lowest 1000m included 19 model levels with the lowest full model level at 19m. Static field data, such as topography and land use index, were provided by the US Geological Survey in a horizontal resolution of 30 arcseconds (0.9km in north-south direction). Initial and lateral boundary conditions were taken from the ECMWF operational analysis data on a 0.125˚ x 0.125˚ horizontal resolution and on 91 vertical levels, and updated every six hours. Sea ice and sea surface temperature (SST) were taken directly from the ECMWF data at the time the simulation started (3 May 2011) and remained fixed during the whole simulation period, assuming full sea-ice coverage for any model grid point with positive sea-ice flag. This approach is justified by the good agreement between the ECMWF sea-ice flag and satellite images of sea-ice coverage on 5 May, both showing dense sea-ice east of Svalbard (Figure 3). Conversely, to the west of Svalbard, sea-ice is absent. Sea surface temperatures are, as usual, higher to the west than east of Svalbard. This is due to the northward flowing warm and saline Atlantic Warm Current (AWC) or 'Gulf stream' that elevates temperatures along Svalbard's west coast (the AWC subsequently sinks below the cold polar waters further north).~~

~~For cloud microphysics the WRF single moment 3-class simple ice scheme (Dudhia, 1989; Hong et al., 2004) was used. Radiation was parameterised with the Rapid Radiative Transfer Model (RRTM) longwave scheme (Mlawer et al., 1997), and the Dudhia shortwave scheme (Dudhia, 1989). Surface fluxes were provided by the Noah Land Surface Model (LSM), a four-layer soil temperature and moisture model with snow cover prediction (Chen and Dudhia, 2001). In the first and second domain, the Kain-Fritsch cumulus scheme (Kain, 2004) was applied in addition, whereas in the third domain, cumulus convection was neglected.~~

~~Sensitivity tests were made with three different boundary layer parameterisation schemes as follows: the Yonsei University (YSU) scheme (Hong et al., 2006) is a non local first order closure scheme that uses a counter gradient term in the eddy diffusion equation, and is the default ABL scheme in WRF. The Mellor-Yamada-Janjic (MYJ) scheme (Janjic, 1990, 1996, 2002) uses the local 1.5 order (level 2.5) closure Mellor-Yamada model (Mellor and Yamada, 1982), where the eddy diffusion coefficient is determined from the prognostically calculated turbulent kinetic energy (TKE). According to Mellor and Yamada (1982), it is an appropriate scheme for stable to slightly unstable flows, while errors might occur in the free convection limit. The Quasi-Normal Scale Elimination (QNSE) scheme (Sukoriansky et al., 2006) is, as the MYJ scheme, a local 1.5 order closure scheme. In contrast to the MYJ scheme, it includes scale dependence by using only partial averaging instead of scale independent Reynolds averaging, and is therefore able to take into account the spatial anisotropy of turbulent flows. It is thus considered especially suited for the stable ABL.~~

The data analysis of this study focuses on balloon flights 4 and 5 that made repeated soundings quantifying as a function of pressure (altitude) the meteorological variables: temperature (T), specific humidity (Q) and northward and eastward winds (V,U). The balloon locations during these flights are shown in Figure 1. A detailed model comparison is made for flight 4 over time-periods 06-12h UTC on 8 May (JD 128) and for the 24hr flight 5 (21-21h UTC) on 10-11 May (JD 130-131).

2.3 Model reanalyses products ERA-I and ASR

The CMET observations are compared to two model reanalyses; ECMWF ERA-Interim (Dee et al., 2011) and the Arctic System Reanalysis (Bromwich et al., 2016). ERA-I (available from http://apps.ecmwf.int/) has approximately 80 km (T255 spectral) resolution on 60 vertical model levels from the surface up to 0.1 hPa, at 6 hrly resolution. The boundary layer and lower troposphere (> ~800 hPa) correspond to 14 model levels. For this study, bi-linearly interpolated model level data was downloaded at 0.125˚ spatial resolution then further linearly interpolated. ASR uses the polar-optimised version of the Weather Research and Forecasting Model (Polar-WRF: Bromwich et al., 2009) with an inner domain that extends over latitudes > 40˚N, using ERA-I output as boundary conditions. ASR (version 2) has 15 km resolution on 70 vertical model levels from the surface up to 0.1 hPa, at 3 hrly resolution (ASR version 1 at

30 km resolution is used in this study only for comparison to a surface station). The boundary layer and lower troposphere (> ~800 hPa) correspond to 30 model levels. For this study, full ASRv2 model level data was made specially available by the ASR team for selected field dates. Pressure-level data for ASRv2 will soon be publically available from http://rda.ucar.edu/. The ASR and ERA-I reanalyses were 4-D (latitude, longitude, pressure and time) interpolated to the CMET balloon for direct comparison. A main difference between these two reanalyses is the much higher temporal (3 hrly) and spatial (15 km) resolution of ASR. This provides a more highly resolved simulation of small-scale meteorological processes (especially within the boundary layer) as well as topography. Another difference is that ASR Polar WRF has non-hydrostatic dynamics whilst ERA-I pressure is hydrostatic. Both model reanalyses include assimilation of remotely sensed retrievals and in-situ surface and upper air data, 4D for ERA-I and 3D for ASR. ASR uses a high resolution land data assimilation system and uses Polar WRF which includes the Noah land surface model and a detailed fractional sea-ice description including extent, concentration, thickness, albedo and snow cover (see Bromwich et al., 2016 for details). For ERA-I surface properties are less detailed (spatially, temporally) than for ASR, but sea-ice is also fractional and updated daily.

Sea-ice concentration in ERA-I and ASR models is shown in Figure 2 for 8^{th} May (JD 128), the date of the CMET flight 4 soundings. Also shown is a satellite image of sea-ice coverage (obtained for 5 May, JD 125). The west of Svalbard is ice-free, consistent with sea-surface temperature in this region (see Introduction), whilst dense sea-ice occurs east of Svalbard. The satellite image also shows some small-scale features ice-free areas (polynyas). These are not seen in the ERA-I ice-field but are represented in ASR as zones of lower ice concentration.

~~3~~2 3 Results and Discussion

~~3.1~~2.1 3.1 Meteorological conditions ~~and ground-stations compared to the WRF simulation~~during the campaign

The period of 3-12 May 2011 was characterized by rapidly changing meteorological conditions, reflected in the different CMET flight paths (Figure ~~1a;b)~~1). The time evolution of the pressure systems driving the winds that advected the CMETs is illustrated by ERA-I model surface pressure maps in Figure 3. The start of the campaign is influenced by a high pressure system that slowly advected balloon 3 northwards. A low pressure system then develops to the north and ~~the 6-hourly averaged~~east of Svalbard, which is responsible for the south-eastwards advection of Balloon 4. Presence of a high pressure system causes a slow northwards followed by eastwards advection of Balloon 5. Surface observations (resolution: minutes) from the AWIPEV meteorological station~~ surface observations shown in Figure 4 (AWIPEV,~~, in Ny-Ålesund~~)~~ (Maturilli et al., 2013) are shown alongside the ERA-I and ~~Supplementary Material S1 (Verlegenhuken, N Svalbard). At first, northerly winds carried cold air to Ny-Ålesund, causing surface temperatures to decline, reaching an hourly minimum of -9.~~ASR model outputs in Figure 4~~ °C~~. Greatest wind-speeds during the campaign are observed on ~~5~~8th-10th May~~. The wind direction then changed to southerly~~ with the AVIPEV station registering a maximum wind-speed of 17.4 m/s around noon on 9 May. During this period the winds ~~over not much more than one day, leading to increasing temperatures and an hourly maximum of 2.9 °C on 6 May. The wind direction subsequently become more~~ became north-westerly ~~and then northerly with high wind-speeds on 8 and 9 May, given occurrence~~due to the presence of a high pressure system SW and a lower pressure system NE of Svalbard~~, and the AVI-PEV station registered a maximum wind-speed of 17.4 m/s around noon on 9 May.~~ . This caused temperature to decrease during this period. This was followed by a period of ~~lowwind~~low wind-speed over 11-12 May, also reflected in the 24 hr CMET flight to the east of Svalbard, with low but increasing temperatures recorded at the ~~Spitsbergen~~ meteorological ~~stations. The WRF simulations~~station. Both models show good general agreement to the ~~6 hourly averaged~~Ny-Ålesund surface meteorological observations ~~at Ny-Ålesund~~of 2m temperature, relative humidity and surface pressure, Figure 4~~, (and Verlegenhuken station in N Svalbard, Figure S1), with similar results for all three ABL schemes. However,~~. This is not entirely unexpected given the ~~high (> 10 m/s) southerly surface winds predicted on 6-7 May for Ny-Ålesund were not observed. Outside of these dates, the model generally~~use of data assimilation in both reanalyses. The models reproduced the ~~winds, albeit at a~~variation in 10m wind~~-~~-speed, but not always the wind-direction ~~30º greater (clockwise) than typically observed in Ny-Ålesund (see wind-roses~~reported at AWI-PEV, Figure ~~S2),~~4. This is likely due to ~~a~~known along-fjord wind ~~channeling effect~~channelling in the Kongsfjorden that ~~is not fully captured by~~ occurs on finer scales than the ~~model. Temperature was well reproduced however somewhat overestimated during cold periods (e.g. 5 and 11-12 May) at both surface stations.~~

~~3.2 Atmospheric boundary layer over Spitsbergen: topography, inversions and low level jets~~

~~The four CMET soundings over Svalbard topography are compared to WRF wind-speed, relative humidity and temperature profiles in Figure 5, for the three different boundary layer schemes. Notably the results using the three ABL schemes are not strongly differing from each other, but collectively show greater disagreement to the observed ABL profiles. WRF captures the profiles with weak winds (profile 1, 4) well, but not on 5-6 May (profile 2, 3) where the CMET observations show the occurrence of a weak low level jet (LLJ) with a wind-speed maximum at around 1200m and lower wind-speeds above and below. WRF in contrast predicts the highest wind-speeds below 1000m and also does not capture the observed inversion above 1300 m. Thus, the model difficulty to predict the lofted altitude of the LLJ appears connected to the model overestimation of surface wind-speed in Ny-Ålesund on 5-6 May (a model-observation discrepancy not found in Verlegenhuken further north in Svalbard). The occurrence of LLJs is likely promoted by the Svalbard topography in conjunction with a stable boundary layer.~~

~~These model-observation discrepancies are consistent with previous studies: Molders and Kramm (2010) found that WRF had difficulties in capturing the full strength of the surface temperature inversion observed during a five day cold weather period in Alaska. Kilpeläinen et al. (2012) found that WRF reproduced only half the observed inversions, and often underestimated their depth and strength, and that the average modeled LLJ was deeper and stronger than that observed. An overestimation of surface wind-speeds by WRF, especially in case of strong winds, has also been reported by Claremar et al. (2012), in comparison to AWS placed on three Svalbard glaciers, and by Kilpeläinen et al. (2011) and Kilpeläinen et al. (2012), in a study of Kongsfjorden. Since low wind-speeds are associated with inversion formation, WRF's overestimation of wind-speed might partly explain the difficulties in capturing (the strength of) inversions (Molders and Kramm, 2010). Consequently, since elevated inversions are often connected to low level jets (Andreas et al., 2000), the difficulties in capturing inversions could help explain the model difficulties in predicting low level jets.~~

~~A likely limitation to the WRF model capability over complex topography is its horizontal and vertical~~ resolution~~. The model set-up used here includes 61 vertical layers, which Mayer et al. (2012b) suggests are necessary to resolve ABL phenomena, such as low level jets. However~~ of the reanalyses. Indeed, Esau and Repina (2012) ~~note~~found that even a ~~model~~

~~resolution of 1 km in the horizontal does not properly represent the valley and steep surrounding mountains in Kongsfjorden, finding that even a~~very fine resolution model (56 x 61 m grid cell~~, 20 times higher than the 1 km grid cell used in this and other WRF studies~~) could not fully resolve near-surface small-scale turbulence in the strongly stratified Kongsfjorden atmosphere~~.~~, where the valley is surrounded by steep mountain topography.

~~3.3 CMET atmospheric profiles east of Spitsbergen: the role of sea-ice~~

~~The two consecutive CMET profiles over sea ice east of Svalbard are compared to WRF model run 2 in Figure 6. All three schemes tend to overestimate wind speed, especially at the low levels. Nevertheless the slope of the wind profile corresponds approximately to the observations. Potential temperature is underestimated by around 2.5K in all schemes. The largest difference between the observations and the model is found at the low levels, where it reaches up to 4K. However, relative humidity is in better agreement, meaning that specific humidity must also be lower in the model than in the observations (e.g. a 4K difference at 85 % RH corresponds to a~~ ~~$9\cdot10^{-4}$ kg/m^3~~ ~~absolute humidity, a difference of around one quarter to one third ambient levels). The temperature and specific humidity bias is most probably due to an over representation of sea ice in the WRF model setup, which exerts a strong control on surface conditions. Even though the sea ice flag from the ECMWF data seems to agree fairly well with satellite sea ice observations (Figure 3), areas of polynyas and leads that can be recognized on the satellite picture were represented as homogeneous sea ice in the model. Further, the 100% sea ice coverage assumed in the model for grid cells with positive sea ice flag may not reflect reality: small patches of open water amongst very close (90%-100%) or close (80-90%) drift ice would promote sea-air exchange, enhancing both temperature and specific humidity at the surface (Andreas et al., 2002).~~

~~Inclusion of fractional sea-ice in WRF (available for WRF version 3.1.1 and higher) might rectify this problem, but is not straightforward to implement: the amount of sea ice in a grid cell varies with time through sea ice formation, break up and drifting, the latter typically a dominant control on ice presence during late spring east of Svalbard. However, the WRF meteorological model does not simulate surface oceanographic processes, thus predicted sea-ice presence depended only on whether the SST was above or below the freezing point of sea-water. An option is to remove excessive sea ice manually, as, e.g., in Mayer et al. (2012b) or to update the sea ice field and the SST at certain intervals (e.g. six hours) with data from observations or re-analyses, as in Kilpeläinen et al. (2012), but this becomes demanding over~~

~~large regions. Nevertheless, given its strong control on ABL processes, a fractional sea ice approach is recommended for future studies, particularly if a longer series of CMET soundings can be achieved, e.g. during balloon flights advected in a pole-ward direction, rather than towards Russia, which necessitated the flight to be terminated on command after only two profiles in our study.~~

~~3.4 Automated CMET soundings during a 24 hr flight west of Spitsbergen~~

3.2 CMET profiles over sea-ice compared to ERA-I and ASR: Temperature inversion

The two consecutive CMET profiles of temperature, specific humidity, U and V winds over sea-ice east of Svalbard (Balloon flight 4) on the morning of JD 128 are compared to 4-D interpolated ERA-I and ASR model data, Figures 5 and 6. The in-flight CMET soundings quantify temperature and humidity profiles that increase towards the surface, as expected, and winds (derived from the balloon flight path) from the north-west. There is good general agreement to ASR and ERA-I. However, the CMET observes a temperature inversion at around 990-970 hPa that persists for most of the sounding time-series. This temperature inversion is captured by ASR in good agreement to the CMET but is not reproduced by ERA-I. ASR finds a strong gradient in humidity related to this inversion barrier, but the CMET observes a more shallow humidity gradient. ERA finds an even shallower gradient in humidity than the CMET. Both models show strengthening westerly winds during the soundings, as observed. The CMET observed a reversal in V winds near the surface (> 1000 hPa). This is better captured by ASR than ERA-I, where it is related in the model to the inversion layer. However, there are differences in V winds at higher altitudes, which are more variable in ASR than in the CMET and ERA-I.

The potential temperature and specific humidity profiles from the CMET flight are further shown in Figure 7, alongside equivalent 4D interpolated model outputs at each CMET latitude, longitude, pressure and time location. The CMET potential temperature profile shows three distinct layers: weakly stable layer at > 990 hPa, a strongly stable layer between 990 and 980 hPa (related to the abovementioned inversion) and stable layer <980 hPa. This agrees well with similar layers identified in the ASR, whereas the absence of an inversion layer in ERA-I leads to a more linear potential temperature profile. The specific humidity profile of ASR shows better agreement to CMET at ~980 hPa where ERA-I overestimates by

0.2 g/kg. At higher altitudes, ERA-I is in better agreement (overestimated by about 0.1 g/kg) whilst ASR shows greater humidity variability (overestimations by up to 0.3 g/kg) than the trend observed by CMET.

It is difficult to infer any temporal trend in the flight 4 CMET profiles over JD 128 morning. The final profile (JD >128.45) shows slightly greater humidity at low altitudes but also slightly lower temperature and the inversion is less clear. ERA-I and ASR show a tendency for increasing surface temperature and humidity. Over the morning ASR predicts deepening layer beneath the inversion, whose top remains at constant height. Unfortunately the experiment could not be continued eastwards into the afternoon as the CMET flight had to be terminated to avoid Russian airspace.

3.3 CMET profiles in coastal area compared to ERA-I and ASR: wind-shear and temperature and humidity trends

Flight 5 provided a series of 18 boundary-layer profiles over a ~~largely~~ sea-ice free region west of Svalbard. With the low wind-speeds (< 5 m/s), the 24 hr balloon trajectory remained relatively close to Svalbard coastline. ~~Figure 7 shows~~ Figures 8 and 9 compare the ~~observed~~along-flight profiles of temperature, specific humidity, U and V winds measured by the CMET to ERA-I and ASR model reanalyses. From morning to afternoon increases in temperature and humidity at the surface are observed by the CMET and shown by both models. Note that the lowest ERA-I model level intersects the CMET sounding at low altitudes (likely due to non-realistic surface topography), preventing model comparison, whereas this problem does not occur for ASR.

Overall there is good agreement between the reanalyses and CMET observations but some differences. During the night of JD 130-131 ERA-I underestimates temperature compared to CMET. This is better reproduced by ASR up until midday on JD 131, although still under-predicted. Both models and the CMET nevertheless show relatively small variations in the temperature profiles at this time. Humidity is well reproduced by ASR during the JD 130-131 night and slightly underestimated by ERA-I. On JD 131 morning ERA-I better reproduces the observed enhanced humidity near the surface than ASR. In ASR the vertical humidity transition is sharper than observed by the CMET and humidity underestimated near the surface. Both ERA-I and ASR capture the observed increase in near-surface temperature and specific humidity up to the mid-afternoon. However, the CMET temperature increase is either stronger or earlier than in the models. These temperature and humidity enhancements are also temporally/spatially more localised for ASR than ERA-I. This leads to closer CMET agreement with ERA-I for mid-afternoon temperature but ASR for humidity. Temperature is underestimated by both models at high altitudes in the JD 131 evening whilst humidity is well reproduced.

There are also differences in the U and V winds between ASR and ERA-I, figure 9. The CMET observes strong V wind-shear on the morning of JD 131. This wind-shear pattern is reproduced by ASR but is not captured by ERA-I. V winds become southerly (from direction) in mid-afternoon in both models, but more localised in ASR leading to better early afternoon model agreement, although ERA-I better reproduces the persistence of northerly winds to higher altitudes observed late on JD 131. Westerly U winds are modelled and observed on the evening of JD 131. ERA-I shows high positive U winds at high altitudes only, whereas ASR shows high positive U winds at all levels.

Closer inspection of the CMET temperature shows some signs of hysteresis in this flight with greater temperatures reached during ascents than descents. This is despite the fast time response of the (aspirated) thermistor. A possible explanation might be heating of the balloon surface by the sun, raising the temperature of the air layer in direct contact with the balloon. This air layer could be transported over the sensor during ascents, but not descent profiles. Nevertheless, measurements made during descent only (> 0.1 m/s vertical descent speed) are consistent with the complete ascent-descent inpotential temperature and specific humidity profiles, Figure 10. These profiles show an overall increase (~5-6 K) in potential temperature observed close to the surface that is reproduced by the models but where ASR underpredicts the temperature rise (~3-4 K) and ERA-I exhibits a potential temperature bias of ~-2 K. The observed trend in specific humidity surface is less clear but with an overall enhancement. ASR specific humidity is in agreement to the CMET on JD 131 morning but is underestimated by up to 0.5 g/kg during the afternoon. ERA-I better captures the afternoon humidity maximum but overestimates midday humidity by 0.5 g/kg. The CMET, ERA-I and ASR flight 5 profiles all show a more stable ABL than found for flight 4.

3.4 CMET soundings in detail: decoupled flows and wind-field estimation

Further analysis of the observations from the CMET flight 5 on JD 131 enables to consider local-scale patterns at higher resolution than the reanalyses. The observed profiles of potential temperature, specific humidity, wind-speed and wind-direction~~,~~ over ~02 – 12.5 UTC (JD 131.08 – 131.52) are shown with interpolated data between the soundings~~.~~ to highlight temporally consistent features, Figure 11. The soundings ranged from approximately 150m to 700m during ~~the first part of the flight (~02 – 12.5 UTC, JD 131.08 – 131.52). Specific humidity is greatest and potential temperature lowest nearer the surface, as expected. Specific~~this period. As mentioned previously, specific humidity tends to increase during the flight, particularly in the lower and middle levels~~, which can be interpreted as a diurnal enhancement from surface evaporation~~. However, beyond JD 131.40 (9.6 UTC) there is actually a decrease in humidity in the lowermost levels, with maximum humidity in the sounding occurring around 350 m altitude. Concurrent to this there is also a small increase in potential temperature at low altitudes. The wind-speed and direction plots indicate relatively calm conditions, with greatest wind-speed in the lower levels generally from a southerly direction. In contrast, at the top of the soundings the balloon encountered winds from a northerly direction, above 600 m. From JD 131.35 onwards, the observed winds became broadly southerly also at 600 m. However, a band of rather more west-south-westerly winds developed at mid-altitudes (~450 m), and low-level winds became (east)-south-easterly from JD 131.4 onwards. ~~An important overall conclusion from these measurements is~~ This indicates that the balloon was not strictly sampling a uniform air-mass during this ~~flight, rather it encountered a variety of~~ period. Whilst previous studies have used CMET's to study Lagrangian air mass trajectories (e.g. Voss et al., ~~properties and behaviours over~~2010), here the ~~course of the soundings. While the complex flow in this case largely precludes a~~ flight path is quasi-Lagrangian~~-type process study,~~. As consequence, the temperature and humidity trends observed along the flight path cannot be wholly interpreted in Lagrangian terms (e.g. tracing of diurnal signature on a single air parcel), rather must also consider the ~~series of profiles none-the-less provides a nuanced understanding that is not possible~~Eularian perspective (e.g. advection of air masses with ~~traditional rawinsondes or constant-altitude balloons.~~distinct properties into and out of the CMET flight path, and their mixing).

~~The CMET observations appear~~The continuous series of CMET vertical profiles provide a more detailed overview on local-scale meteorology than is possible with traditional rawinsondes or constant-altitude balloons. The CMET observations are consistent with the occurrence of a low-level flow that is decoupled from higher altitudes, and – at least initially ~~– a diurnal~~an increase in surface humidity~~ through enhanced ocean evaporation.~~. The ~~observed wind shear is consistent with a tilted high pressure system (that tilts with altitude~~

~~towards the west of Svalbard, according to the WRF model), whilst~~ surface winds may be ~~further~~ influenced by low-level channel flows. An outflow commonly exits~~–~~ from nearby Kongsfjorden-Kongsvegen valley (e.g. Esau and Repina, 2012) but is hard to identify from the ground-station in Ny Ålesund (south side of Kongsfjorden) given the rather low wind-speeds during this period. ~~–~~Winds that originate over land are likely colder, with lower humidity than marine air masses. Thus, the CMET observations of lower specific humidity between JD 131.40 – 131.5 (9.6- 12 UTC) might be explained by fumigation from or simply sampling of such a channel outflow. Alternatively, the CMET's location ~~over~~near Kapp Mitra Penninsula at this time may indicate an even more local source of dry air impacting low levels. A final possibility could be overturning of air masses in the vertical, bringing less humid air, with higher potential temperature to lower altitudes. At mid-levels (~450 m) a relatively humid air layer persists, properties which suggest it likely has origins from the surface. It appears to be advected north-eastwards, potentially replenishing air over Svalbard to replace that which may be lost from the channel outflow. ~~Further discussion is provided in conjunction with the WRF model results.~~

~~The CMET observations are compared to WRF model output at two time-periods, UTC 07h and 15h on 11 May (JD 131.3 and 131.6, respectively). Model output (in 2D) is presented in two ways: (i) cross-sections of relative humidity (RH) and potential temperature with altitude along a transect in the WRF model (QNSE, YSU and MYJ schemes) that lies in an approximately S-N direction and is reasonably close to (but not identical to) the balloon flight path, see Figure 8; (ii) maps of temperature and absolute humidity (kg/kg) at a constant model layer (equivalent to ~ 300m asl over the oceans although reaching higher altitudes over the Svalbard terrain) that provide a geographic spatial context. For clarity, only output from WRF MYJ BL scheme is illustrated (see Supplementary Material for QNSE and YSU schemes).~~

~~For (i), the WRF model temperature and humidity cross-sections at 07h and 15h are shown alongside CMET observations along the whole balloon flight, in Figure 9 and 10, respectively, and where the balloon locations at 07h and 15h are denoted by a triangle or cross, respectively. The model generally agrees with the balloon observations: potential temperature increases with altitude, and surface temperature decreases with increasing latitude in the 07h cross-section. Boundary layer height is denoted by a sharp humidity decrease, at approx. 600 m (declining to 400 m at higher latitudes) in the 07h WRF cross-section. For all the model schemes, a greater relative humidity and a higher boundary layer is predicted in the~~

~~15h cross-section, as expected from the diurnal cycle, whereby solar heating increases evaporation to enhance RH, and increases thermal buoyancy to enhance ABL height. By 15 h, the model potential temperature is also generally higher, however, surface temperatures now increases with latitude. This may reflect greater solar heating experienced at higher Arctic latitudes in the spring.~~

~~This overall RH trend of the model is in agreement to the observations: the CMET balloon data also exhibits a higher relative humidity at 15 h than 07h. There is also some variability between the different model boundary layer schemes: for the 15 h cross-section boundary layer height, YSU > QNSE > MYJ in terms of both relative humidity and ABL height. However, diurnal variability is not the only control on ABL humidity (as discussed above). The geographical influence is illustrated by (ii); spatial maps of absolute humidity across a model layer (corresponding to ~300m asl over oceans, somewhat higher over land) in Figure 11. As expected, humidity in the marine air in the ice-free coastal region is greater than over Spitsbergen land, where temperatures were below freezing (see AWIPEV station time-series Figure 4). Mixing or transfer between the marine- and land-influenced air masses can thus exert a significant influence on the observations, consistent with the findings from the CMET analysis above. The model results presented at 07 and 15 h clarify this influence in a geographic context. Between launch and 7am the CMET moved into a more marine environment thus humidity increased. The balloon then moved northwards, perhaps drawn by a channel outflow from Kingsbay. Over this period humidity is constant or declining slightly, as the balloon passes across Kongsfjorden Bay and over the Kapp Mitra peninsula. From ~midday to 15h the humidity increases again as the balloon travels northwards (a temporary westerly diversion occurs following blocking of the low-level flow by Svalbard terrain). This humidity enhancement appears mostly caused by the diurnal effects of enhanced evaporation. Alternatively, simple transport of the balloon into or air-mass mixing with moister marine air could play a role, but in any case the diurnal humidity signal appears strong across this NW region. After 15h the balloon was raised to higher altitudes hence the humidity decreased compared to that in the fixed model level (a similar decrease can be seen in the model altitude-transect plots, Figure 10).~~

~~Finally, we return to the subject of the quasi-Lagrangian nature of the CMET balloon flight. A detailed analysis is beyond the scope of this study, nevertheless the wind, humidity and temperature observations indicate presence of more than one air mass in this coastal region.~~

~~Whilst CMETs have previously been used in Lagrangian-type experiments to track the evolution of an airmass (e.g., Voss et al, 2010), this case-study presents more complex atmospheric conditions. Both vertical winds and horizontal wind-shear can affect the Lagrangian nature of the CMET balloon experiment. Vertical air mass movement is not measured by the CMET payload but is estimated by the WRF model to be sufficiently low (typically << 0.01 m/s) to be negligible in most cases, with the exception of localized areas in QNSE scheme (see Supplementary Material, Figure S4). The CMET balloon movement was itself used to determine horizontal winds (Figure 7), and showed decoupled air flows of near opposite direction in the morning of 11 May (southerly winds at low altitudes, northerly winds at higher levels). Balloon soundings that traverse these layers will thus influence its overall trajectory. Trajectories were estimated from the observed winds at 50 m altitude intervals.~~Wind-fields are estimated from the CMET balloon 5 flight path for an 8-hour period starting in the early morning of 11 May (JD 131), Figure 12. As per previous figures, the CMET balloon movement during the soundings has been used to estimate wind-speed and direction. Here, wind-trajectories are derived from the observed winds at 50 m altitude intervals for each up or down profile. The trajectory vectors (of length proportional to the wind-speed × time elapsed between soundings) are placed end-to-end to estimate the wind-field, shown in Figure 15 (gray mesh) alongside the CMET flight (red). This approximate technique assumes horizontally uniform flow (in the vicinity of the balloon and computed trajectories~~) during the 8-hour period starting in the early morning of 11 May, Figure 12.~~). The lowermost layer exhibited greatest wind-speed thus has the longest (and least certain) trajectory, approximately double that of the balloon during the same period. The uppermost layer flows southwards before reversing direction, approximately returning to its initial position~~.~~ at 600 m altitude. The middle layer trajectory is quite similar to that of the overall CMET balloon flight, but is transported initially somewhat more westwards, and later somewhat more eastwards, due to the ESE winds experienced in the late morning (see Figure ~~7~~11). It is worth noting this final direction mirrors findings from two of the other CMET ~~flights~~balloons, whose ~~initial~~flight paths out of Kongsfjorden deviated to the north-east into the nearby Krossfjorden~~. While the~~, Figure 1. These balloon-based trajectories ~~and repeating profile measurements are not Lagrangian, they do~~ provide insight into the complex local dynamics of low-altitude circulation influenced by complex terrain. Furthermore, the trajectories and profile data can be computed and displayed in near-real time, ~~allowing future experiments~~ to ~~be modified during~~ inform the real-time in-flight decisions on CMET altitude control (e.g~~.,~~. to track specific layers or events~~). Such experiments can provide observational insights that help constrain the complex meteorology.~~ of meteorological interest).

3.5 Discussion: ASR and ERA-I model reanalyses in comparison to CMET

Both reanalyses showed good general agreement to the CMET flights, finding more stable conditions for flight 4 (over sea-ice) than flight 5 (coastal). For flight 4: ASR showed a better capability than ERA-I to reproduce a temperature inversion observed over sea-ice. ASR and ERA-I broadly reproduced the enhanced humidity near the sea-ice surface but showed some discrepancies with the CMET in the vertical-spatial distributions. For flight 5: ASR better reproduced observed wind-shear near to Svalbard coast. Both models exhibit increasing specific humidity and temperature in the near-surface atmosphere from morning to afternoon on JD 131, in agreement to the trend observed. However, compared to the CMET the surface temperature and humidity enhancements were under-predicted by ASR. ERA-I underestimated ABL temperature. Whilst increasing humidity and temperature over the daytime might be expected based on the diurnal cycle, Section 3.4 highlights the quasi-Lagrangian nature of flight 5 that also requires consideration of air-mass advection and mixing. Figure 13 presents ERA-I (regional-scale) and ASR (local-scale) pattern in surface 2m temperature and humidity for the duration of JD 131, alongside the CMET flight path. A zone of warm and humid air initially to the south-west of Svalbard advects northwards and eastwards. This likely exerted a significant influence on the observed and modelled along-flight surface trends. The ASR also clearly shows local diurnal influences on surface meteorology, particularly on 2m temperature over the elevated topography east of the flight.

The temperature and humidity increases along flight 5 are temporally-spatially broader for ERA-I than for ASR (Figure 8). This may to some degree reflect model diffusion on the larger ERA-I grid-size ~80 km compared to 15 km for ASR). The poorer ERA-I resolution of Svalbard topography will also affect simulated meteorology in this coastal area, where there may be local mixing, e.g. between marine and land-influenced air masses. A major contributing factor to ASR performance in capturing observed wind-shear (flight 5) and temperature inversion (flight 4) and is likely the higher vertical model resolution of ASR compared to ERA-I, with ASR having about double the number of model levels than ERA-I at > 800 hPa, see Methods for descriptions. This improves the representation of the shallow polar ABL with its distinct layers. Noting that higher resolution models that better capture spatial patterns can nevertheless lead to worse agreement to observations due to slight spatial shifts (Wesselen et al., 2014), we choose not to reduce the ERA-I, ASR, and CMET comparison to standard metrics (e.g. a correlation coefficient) here. The representations of Arctic air-sea-ice interaction and parameterisation of turbulence fluxes in the boundary layer schemes will also influence the model outputs (e.g. Mölders and Kramm, 2010), but are difficult to assess from this study. In future, campaigns where multiple CMET balloons are sequentially co-launched to horizontally and vertically and probe an atmospheric region combined with model sensitivity simulations to test the different processes and model boundary layer schemes could provide this insight.

43 4 Conclusions

Five Controlled Meteorological (CMET) balloons were launched from Ny-Ålesund, Svalbard on 5-12 May 2011, to measure in-situ the meteorological conditions (~~RH~~humidity, temperature, ~~wind-speed) over Spitsbergen and~~ winds, pressure) in the surrounding Arctic region. ~~Analysis of~~Repeated soundings were performed along the ~~meteorological data, in conjunction with simulations using the Weather and Research Forecasting (WRF) model at high (1 km) resolution provide insight~~CMET flights that probed into ~~processes governing~~ the Arctic atmospheric boundary layer ~~and its evolution~~. The CMET data are analysed in comparison to model output from the ERA-Interim and Arctic System reanalyses.

~~Three ABL parameterizations were investigated within the WRF model, YSU (Yonsei University), MYJ (Mellor-Yamada-Janjic) and QNSE (Quasi-Normal Scale Elimination). These schemes showed closer similarity to each other than between the model runs and the observations. This indicates more fundamental challenges to mesoscale modelling~~CMETs are a novel balloon technology capable of multi-day flights in the ~~Arctic, as identified from this study to include (i) the occurrence of inversions and low level jets over Svalbard topography~~troposphere and performing in ~~association with stable boundary conditions, which likely can only be captured at greater model resolution (ii) the presence of (fractional) sea-ice that acts to modify sea-air exchange, but whose dynamical representation in the model is not straight-forward to implement.~~

~~The WRF model simulations showed good general agreement to surface meteorological parameters (temperature, wind-speed, RH) in Ny-Ålesund and Verlegenhuken, N-Svalbard over 03-12 May, 2011. However, temperatures were somewhat underestimated during colder~~

~~periods, and surface winds were severely overestimated on 5-6 May in Ny Ålesund. Comparison of four CMET profiles over Svalbard topography to the WRF model indicated model difficulties in capturing inversion layers and a low-level jet (LLJ). The CMET observations thereby provided a context for the predicted high surface wind speeds in Ny Ålesund, which were observed aloft but not at the surface during the campaign. A higher resolution is likely required to improve the model ability to simulate the small-scale atmospheric dynamics particularly for stable Arctic boundary layer conditions combined with Svalbard topography.~~

~~Two CMET~~ flight soundings ~~also probed~~on command. Five CMET balloons were launched in May 2011. Balloons 1 and 2 had only short flights whilst balloon 3 made multi-day flight to the north but did not perform any soundings. Flights 4 and 5 made repeated soundings that profiled the ABL. CMET balloon 4 made two soundings into the boundary layer over sea-ice to the east of Svalbard~~, during a balloon flight which despite~~. Despite good performance this flight needed to be terminated to avoid encroaching on Russian territory. ~~Model biases in wind speed and surface level temperature (and inferred for specific humidity) over this region are likely due to the representation of sea-ice in the model. Whilst the ECMWF-derived sea-ice flag used appears reasonable, the presence of fractional sea-ice east of Svalbard may have enabled greater air-sea exchange of heat and moisture than predicted by the model, which assumed 100 % sea-ice coverage for positive sea-ice flag. Fractional representation of sea-ice in WRF is thus desirable, but is not straightforward to implement as sea-ice coverage depends on both sea-surface temperature driven freezing/melting processes and ocean-current driven advection, the latter being dominant East of Svalbard during spring. Improved sea-ice representation (e.g. applying a manual correction every 6 h) is recommended for future studies especially if multiple soundings over sea-ice during longer duration CMET flights (i.e. northerly rather than easterly advected) can be achieved.~~

~~A series of continuous~~ CMET balloon 5 was placed in an automated soundings ~~was performed during a CMET flight over a sea-ice free region west of Svalbard, tracing atmospheric boundary layer temperature and relative humidity profiles~~mode and made a suite of 18 continuous soundings along the ~~flight and with altitude. Meteorological conditions encountered were complex, including a low-level flow decoupled from the air mass at higher altitudes. An increase in low-level relative humidity was observed, consistent with diurnal enhancement expected from evaporation. The WRF model predicted both an increase in RH~~

~~and ABL height over the diurnal cycle concurrent with the CMET observations. The data-model interpretation also considers influence of air masses of different origin which augment the diurnal trends: air masses originating over the warm saline ocean waters have typically greater humidity than over the cold Svalbard topography.~~

~~Finally, the semi-Lagrangian nature of CMET flights is discussed. In this ABL study the balloon likely sampled different air masses through vertical soundings undertaken during the~~north-west coast of Svalbard, during a 24 hr flight~~, under conditions of strong vertical wind-shear. Analysis of the observed wind-fields provides an indication of the balloon trajectory in the context of surrounding wind trajectories at different altitudes~~. To our knowledge, this was the first automated sounding sequence made by a free balloon.

This study focuses on the two flights that performed repeated profiling into the boundary layer. Overall both observations and models identify the ABL was more stable for flight 4 (over sea-ice) than flight 5 (coastal). To the east of Svalbard (flight 4), the observed temperature and humidity increases towards the surface are generally well reproduced by ERA-I and ASR. The CMET observed a temperature inversion over sea-ice which was reproduced by ASR but was not captured by ERA-I. ASR and ERA-I broadly reproduced the enhanced humidity near the sea-ice surface but showed some discrepancies with the CMET in the vertical-spatial distributions. The CMET flight 5 along the north-west coast of Svalbard observed increases in near-surface humidity and temperature, and strong wind-shear. Detailed analysis of the CMET data identifies a low-level flow and provides an estimate of local wind-fields. The wind-shear was captured by ASR but not ERA-I. Both model reanalyses find increasing specific humidity and temperature near the surface, from morning to afternoon on JD 131. The enhancements are more temporal-spatially localised in ASR than ERA-I. The temperature enhancement was under-predicted by ASR whilst ERA-I underestimated ABL temperature. The higher vertical and horizontal resolution of the ASR enables to capture features (temperature inversion, wind-shear) that are not described by ERA-I. However, there are other aspects of the model-observation comparison that are in better agreement for ERA-I than ASR. This might be due to the different representations of processes in the model and could be investigated in future by deploying a suite of CMET balloons over a region combined with model sensitivity studies.

In summary, CMET balloons provide a novel technological means to profile the remote Arctic ~~boundary layer~~ over multi-day flights, including the capacity to perform

~~multiple~~continuous automated soundings~~. CMET capabilities~~ into the atmospheric boundary layer. CMETs are thus highly complementary to other Arctic observational strategies including fixed station, free and tethered balloons, meteorological masts and RPAS/UAVs~~.~~ (drones). Whilst RPAS/UAVs offer full 3D spatial control for obtaining the meteorological observations, their investigation zone is generally limited to tens of kilometers based on both range and regulatory restrictions. CMETs flights provide a relatively low-cost approach to observing the boundary layer at greater distances from the launch site (e.g. tens to hundreds of km), at tropospheric altitudes potentially all the way down to the surface, and more remote from the disturbances of Svalbard topography~~. Analysis of the CMET observations along with output from a regional model output provides insights into the processes that control the observed evolution of meteorological parameters and that pose a challenge to mesoscale simulations of the Arctic atmosphere.~~, for quasi-Lagranian and long-range transport and process studies..

Acknowledgements

This research was sponsored by the Research Council of Norway and the Svalbard Science Forum. We are very grateful to the joint French-German Arctic Research Base AWIPEV in Ny-Ålesund for logistical support, and Anniken C. Mentzoni for fieldwork assistance. PV also acknowledges Smith College for support. TJR acknowledges NSINK, an Arctic Field Grant, CRAICC, and the VOLTAIRE LABEX (VOLatils-Terre Atmosphère Interactions – Ressources et Environnement) ANR-10-LABX-100-01 (2011–20) for funding. ~~PV acknowledges Smith College for support.~~ This study occurred at the end of the Coordinated Investigation of the Climate-Cryosphere Interactions (CICCI) initiative. We are extremely grateful to the ASR team for providing model level ASRv2 reanalysis data in advance of public distribution. We thank Chi-Fan Shih for help in access to the ASR files and David Bromwich for useful comments on the manuscript.

References

~~Andreas E. L., Claffey K. J., and Makshtas A. P.: Low-level atmospheric jets and inversions over the western Weddell sea. Boundary-Layer Meteorology, 97:459–486, 2000.~~

Andreas, E. L., Guest P.S, Persson P.O.G., Fairall C.W., Horst T. W., Moritz R. E., and Semmer S. R.: Near-surface water vapor over polar sea ice is always near ice saturation, Journal of Geophysical Research: Oceans (1978–2012) 107, no. C10: SHE-8, 2002.

Bromwich, D. H., A. B. Wilson, L. Bai, G. W. K. Moore, and P. Bauer, 2016: A comparison of the regional Arctic System Reanalysis and the global ERA-Interim Reanalysis for the Arctic. Q. J. R. Meteorol. Soc., 142, 644-658, doi: 10.1002/qj.2527.

Bromwich D. H., Hines K. M., and Bai L.-S.: Development and testing of polar weather research and forecasting model: 2. Arctic Ocean., J. Geophys. Res., 114:D08122, 2009.

~~Chen F. and Dudhia J.: Coupling an advanced land-surface/ hydrology model with the Penn State / NCAR MM5 modeling system. part i: Model description and implementation. Mon. Wea. Rev., 129:569–585, 2001.~~

~~Claremar B., Obleitner F., Reijmer C., Pohjola V., Waxeg A., Karner F., and Rutgersson A.: Applying a mesoscale atmospheric model to svalbard glaciers. Advances in Meteorology, 22 pages, Article ID 321649, 2012.~~

~~Dudhia J.: Numerical study of convection observed during the winter monsoon experiment using a mesoscale two-dimensional model. J~~Dee DP, Uppala SM, Simmons AJ, Berrisford P, Poli P, Kobayashi S, Andrae U, Balmaseda MA, Balsamo G, Bauer P, Bechtold P. The ERA-Interim reanalysis: Configuration and performance of the data assimilation system. Quarterly Journal of the Royal Meteorological Society. 2011 Apr 1;137(656):553-97.

~~; Atmos. Sci., 46:3077–3107, 1989.~~

Esau I. and Repina I.: Wind Climate in Kongsfjorden, Svalbard, and Attribution of LeadingWind DrivingMechanisms through Turbulence-Resolving Simulations, Advances in Meteorology, Article ID 568454, 16 pages, doi:10.1155/2012/568454., 2012.

Hole L. R., Bello A. P., Roberts T. J., Voss P. B., ~~Hines K. M. and Bromwich D. H.: Development and testing of polar weather research and forecasting (wrf) model. part i: Greenland ice sheet meteorology*. Mon. Wea. Rev., 136:1971–1989, 2008.~~

~~Hong S. Y., Dudhia J., and Chen S. H.: A revised approach to ice microphysical processes for the bulk parameterization of clouds and precipitation. Mon. Wea. Rev., 132:103 120, 2004.~~

~~Hong S. Y., Noh Y., and Dudhia J.: A new vertical diffusion package with an explicit treatment of entrainment processes. Mon. Wea. Rev., 134:23182341, 2006.~~

~~Janjic Z. I.: The step-mountain coordinate: physical package. Mon. Wea. Rev., 118: 1429 1443, 1990.~~

~~Janjic, Z. I.: The surface layer parameterization in the NCEP Eta Model. World Meteorological Organisation publications, WMO TD, 4-16, 1996.~~

~~Janjic Z. I.: Nonsingular implementation of the Mellor-Yamada level 2.5 scheme in the NCEP meso model. NCEP office note 437, 61, 2002.~~

~~Kain J. S.: The Kain-Fritsch convective parameterization: An update. J. Appl. Meteor., 43:170 181, 2004.~~

Vihma T. Measurements by controlled meteorological balloons in coastal areas of Antarctica, Antarctic Science, in press 2016, doi:10.1017/S0954102016000213.

Kilpeläinen T., Vihma T., and Olafsson H.: Modelling of spatial variability and topographic effects over arctic fjords in svalbard. Tellus A, 63(2):223–237, 2011.

Kilpeläinen T., Vihma T., Manninen M., Sjöblom A., Jakobson E., Palo T., and Maturilli M.: Modelling the vertical structure of the atmospheric boundary layer over Arctic fjords in Svalbard. Q. J. R. Meteorol. Soc., 2012.

~~Livik G.: An observational and numerical study of local winds in kongsfjorden, Spitsbergen, Master Thesis at the University of Bergen, 2011.~~

Mäkiranta E., Vihma T., Sjöblom A., and Tastula E.-M.: Observations and modelling of the atmospheric boundary layer over sea-ice in a svalbard fjord. Boundary-Layer Meteorology, 140:105–123, 2011.

Maturilli M, Herber A, König-Langlo G. Climatology and time series of surface meteorology in Ny-Ålesund, Svalbard. Earth System Science Data. 2013 Apr 12;5(1):155-63.

Mayer S., Sandvik A., Jonassen M., and Reuder J.: Atmospheric profiling with the UAS SUMO: a new perspective for the evaluation of fine-scale atmospheric models. Meteorology and Atmospheric Physics, 116:15–26, 2012a.

Mayer S., Jonassen M., A. Sandvik, and J. Reuder. Profiling the arctic stable boundary layer in Advent Valley, Svalbard: Measurements and simulations. Boundary-Layer Meteorology, 143:507–526, 2012b.

~~Mellor G. L. and Yamada T.: Development of a turbulence closure model for geophysical fluid problems. Rev. Geophys. Space Phys., 20:851–875, 1982.~~

~~Mentzoni A. C: Flexpart validation with the use of CMET balloons, Master Thesis at the University of Oslo, 2011.~~

~~Mlawer E. J., Taubman S. J., Brown P. D., Iacono M. J., and Clough S. A.: Radiative transfer for inhomogeneous atmospheres: Rrtm, a validated correlated-k model for the longwave. J. Geophys. Res., 102:16663–16682, 1997.~~

Mölders N. and Kramm G.: A case study on wintertime inversions in interior Alaska with WRF. Atmospheric Research, 95(23):314–332, 2010.

Moore, G. W. K., I. A. Renfrew, B. E. Harden, and S. H. Nernild: The impact of resolution on the representation of southeast Greenland barrier winds and katabatic flows. Geophys. Res. Letts., 42, doi: 10.1002/2015GL063550, 2015.

Moore, G. W. K., D. H. Bromwich, A. B. Wilson, I, Renfrew, and L. Bai. Arctic System Reanalysis improvements in topographically-forced winds near Greenland. Q. J. R. Meteorol. Soc., doi: 10.1002/qj.2798, in press 2016

Persson P. O. G., Fairall C. W., Andreas E. L., Guest P. S., and Perovich D. K.: Measurements near the atmospheric surface flux group tower at sheba: Near-surface conditions and surface energy budget. J. Geophys. Res., 107:8045–8079, 2002.

Riddle E. E., Voss P. B., Stohl A., Holcomb D., Maczka D., Washburn K., and Talbot R. W.: Trajectory model validation using newly developed altitude-controlled balloons during the international consortium for atmospheric research on transport and transformations 2004 campaign. J. Geophys. Res., 111:D23S57, 2006.

Rinke A., Dethloff K., Cassano J., Christensen J., Curry J., Du P., Girard E., Haugen J.-E., Jacob D., Jones C., Kltzow M., Laprise R., Lynch A., Pfeifer S., Serreze M., Shaw M., Tjernstrm M., Wyser K., and Agar M.: Evaluation of an ensemble of Arctic regional climate models: spatiotemporal fields during the sheba year. Climate Dynamics, 26:459–472, 2006.

~~Skamarock W., Klemp J., Dudhia J., Gill D., Barker D., Duda M~~Smedsrud LH, Esau I, Ingvaldsen RB, Eldevik T, Haugan PM, Li C, Lien VS, Olsen A, Omar AM, Otterå OH, Risebrobakken B. The role of the Barents Sea in the Arctic climate system. Reviews of Geophysics. 2013 Sep 1;51(3):415-49.

~~. H. X. Y., and Wang W.: A description of the advanced research WRF version 3, NCAR 451 Tech. Note NCAR/TN-475+ STR, 113 pp. 452, 2008.~~

Stenmark, A., L. R. Hole, P. Voss, J. Reuder, and M. O. Jonassen (2014), The influence of nunataks on atmospheric boundary layer convection during summer in Dronning Maud Land, Antarctica, J. Geophys. Res. Atmos., 119, doi:10.1002/2013JD021287.

~~Stohl A., Wotawa G., Seibert P., and Kromp-Kolb H.. Interpolation errors in wind fields as a function of spatial and temporal resolution and their impact on different types of kinematic trajectories. J. Appl. Meteorol., 34:2149–2165, 1995.~~

~~Stohl A., Hittenberger M., and Wotawa G.. Validation of the lagrangian particle dispersion model flexpart against large-scale tracer experiment data. Atmospheric Environment, 32(24):4245–4264, 1998.~~

~~Sukoriansky S., Galperin~~Tjernström, M, Leck, C, Birch, CE, Brooks, IM, Shupe, MD, Persson, POG, Wheeler, CR, Shupe, MD, Persson, POG, Sedlar, J, Mauritsen, T, Paatero, J and Szczodrak, M (2012) Meteorological conditions in the central Arctic summer during the Arctic Summer Cloud Ocean Study (ASCOS). Atmospheric Chemistry and Physics, 12 (15). 6863 - 6889. ISSN 1680-7316.

Vihma T, Lüpkes C, Hartmann J, Savijärvi H: Observations and modelling of cold-air advection over Arctic sea ice in winter. Boundary-Layer Meteorol 117:275–300, 2005.

~~B., and Perov V.. A quasi-normal scale elimination model of turbulence and its application to stably stratified flows. Nonlinear Processes in Geophysics, 13:9–22, 2006.~~Vihma, T., Pirazzini, R., Fer, I., Renfrew, I., Sedlar, J., Tjernström, M., Lüpkes C., Nygard T.,Notz D., Weiss J., Marsan D., Cheng B., Birnbaum G., Gerland S., Chechin D., and Gascard J. C.: Advances in understanding and parameterization of small-scale physical processes in the marine Arctic climate system: a review. Atmos. Chem. Phys., 14, 9403-9450, 2014.

Voss P. B., Zaveri R. A., Flocke F. M., Mao H., Hartley T. P., DeAmicis P., Deonandan I., Contreras-Jiminez G., Mart´ınez-Antonio O., Figueroa Estrada M., Greenberg D., Campos T. L., Weinheimer A. J., Knapp D. J., Montzka D. D., Crounse J. D., Wennberg P. O., Apel E., Madronich S., and de Foy B.: Long-range pollution transport during the milagro-2006 campaign: a case study of a major mexico city outflow event using free-floating altitude-controlled balloons. Atmos. Chem. Phys., 10:7137–7159, 2010.

Voss P. B., Hole, L. R. Helbling E., and Roberts T. J:. Continuous in-situ soundings in the Arctic boundary layer: A new atmospheric measurement technique using controlled meteorological balloons. Journal of Intelligent & Robotic Systems, pages 1–9, 2012.

Wesslén C., M. Tjernström, D. H. Bromwich, G. de Boer, A. M. L. Ekman, L.-S. Bai, and S.-H. Wang. The Arctic summer atmosphere: An evaluation of reanalyses using ASCOS data. Atmos. Chem. Phys.,

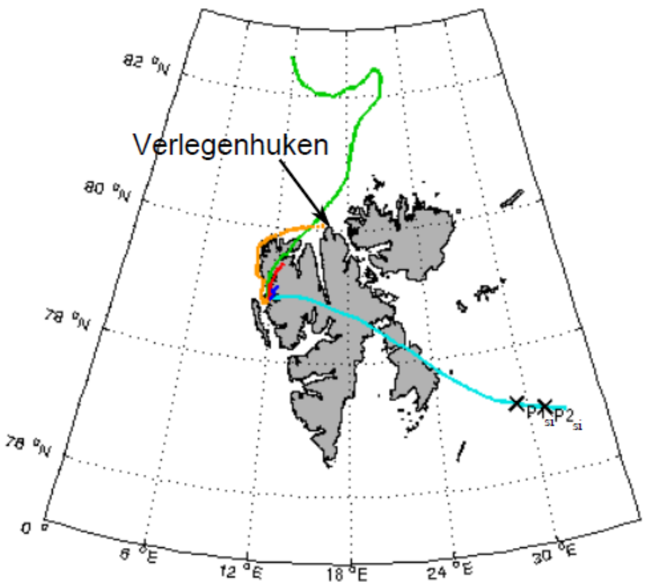

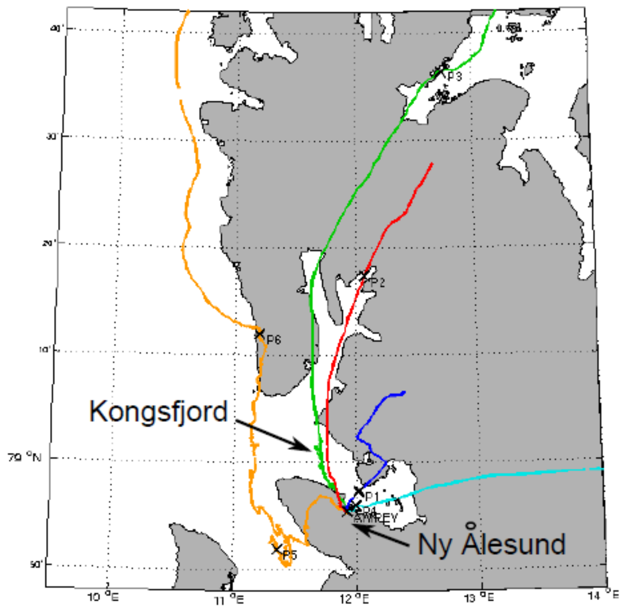

14, 2605-2624, doi:10.5194/acp-14-2605-2014, 2014.

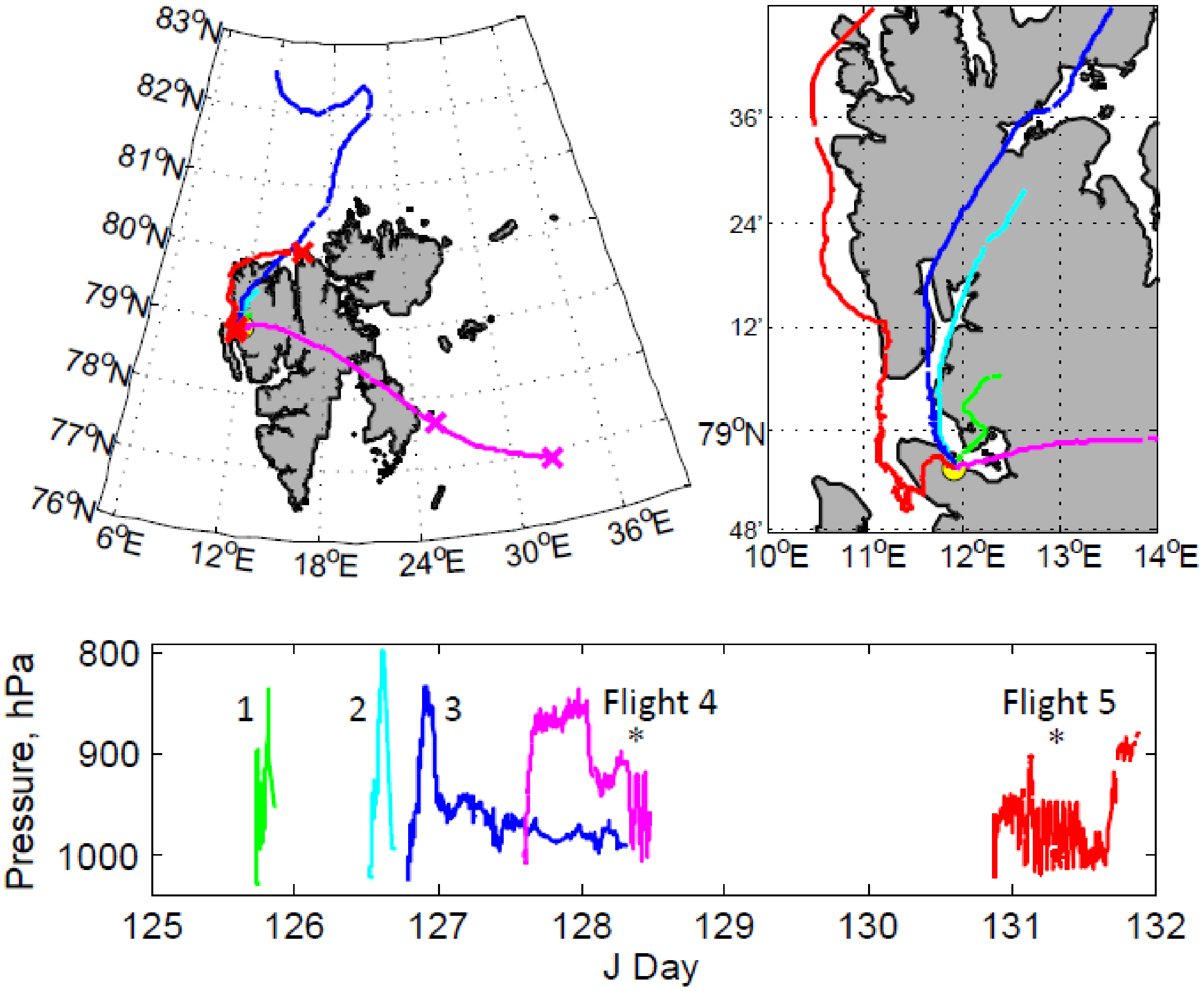

Figure 1~~.~~

Trajectories of five CMET balloons launched from Ny-Ålesund in May 2011. ~~Soundings used for comparison to WRF~~Flight paths are ~~labelled P1si, P2si (over sea-ice east of~~shown on the regional scale of Spitsbergen Island, Svalbard ~~for comparison to WRF model run 2), and P1, P2, P3, P4 (over Svalbard topography for comparison to WRF model run 1). P5~~ and ~~P6 denote balloon locations at 03h and 12h UTC during flight 5 whilst the balloon made automated continuous soundings to~~on the ~~west of Svalbard.~~

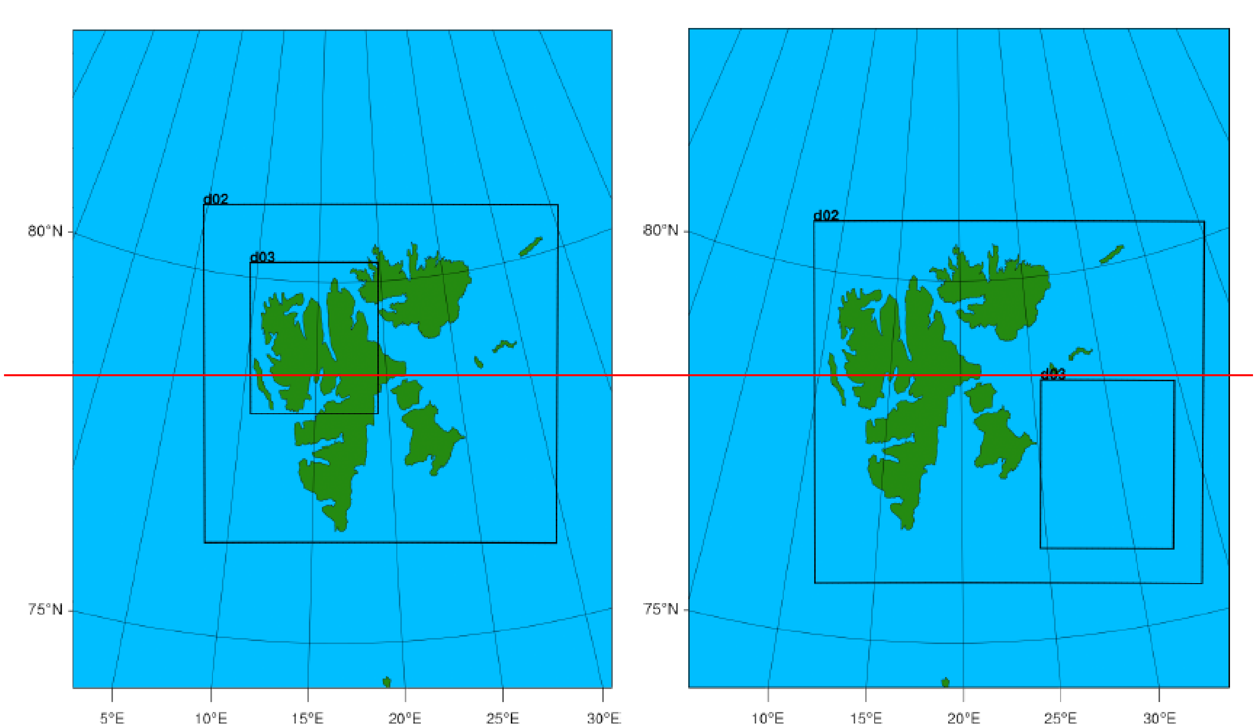

local scale~~Figure 2.~~ of Kongsfjord. Ny Ålesund is maked by a yellow circle and lies at the south side of Kongsfjord. Balloons 4 and 5 performed repeated soundings as shown by the pressure variations in time (marked ‘*’). Analysis periods for flights 4 (06- 12 UTC) and 5 (full flight) are denoted by ‘x’.

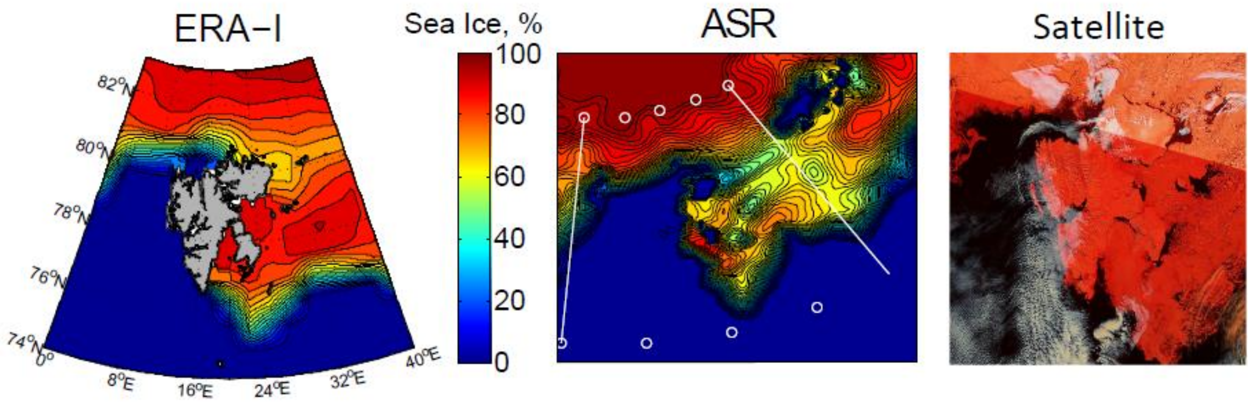

Figure 2. ~~Nested grids of the WRF model setup for the two model runs.~~

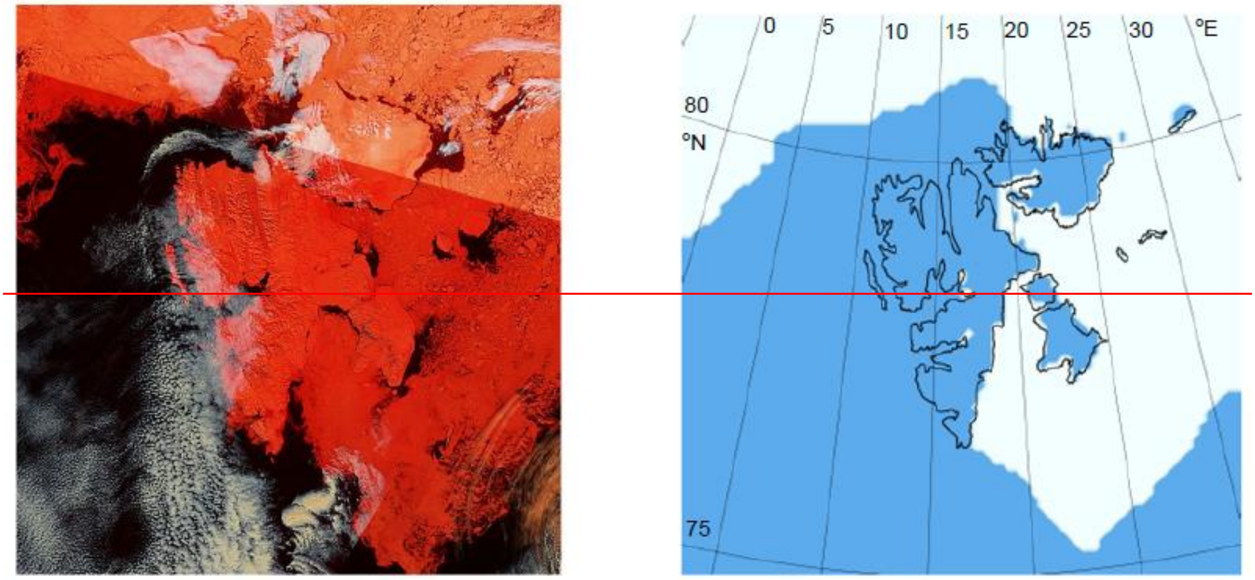

~~Figure 3. Comparison of sea~~Sea-ice ~~conditions around~~concentration field on 8th May (JD 128) in ERA-I and ASR reanalyses. The ERA-I image shows a map of Svalbard ~~(left) to sea-ice flag in WRF model (right).~~overlain. The ERA-I map coordinates are depicted on the ASR image for ease of comparison. Also shown is the Lance rapid response image (right) from the MODIS satellite (downloaded from http://lance-modis.eosdis.nasa.gov/, land and sea-ice are shown in red, cloud cover in white) for 5 May, 2011 ~~and the ECMWF sea-ice flag as used in the WRF model (white = 1, blue = 0).~~(JD 125).

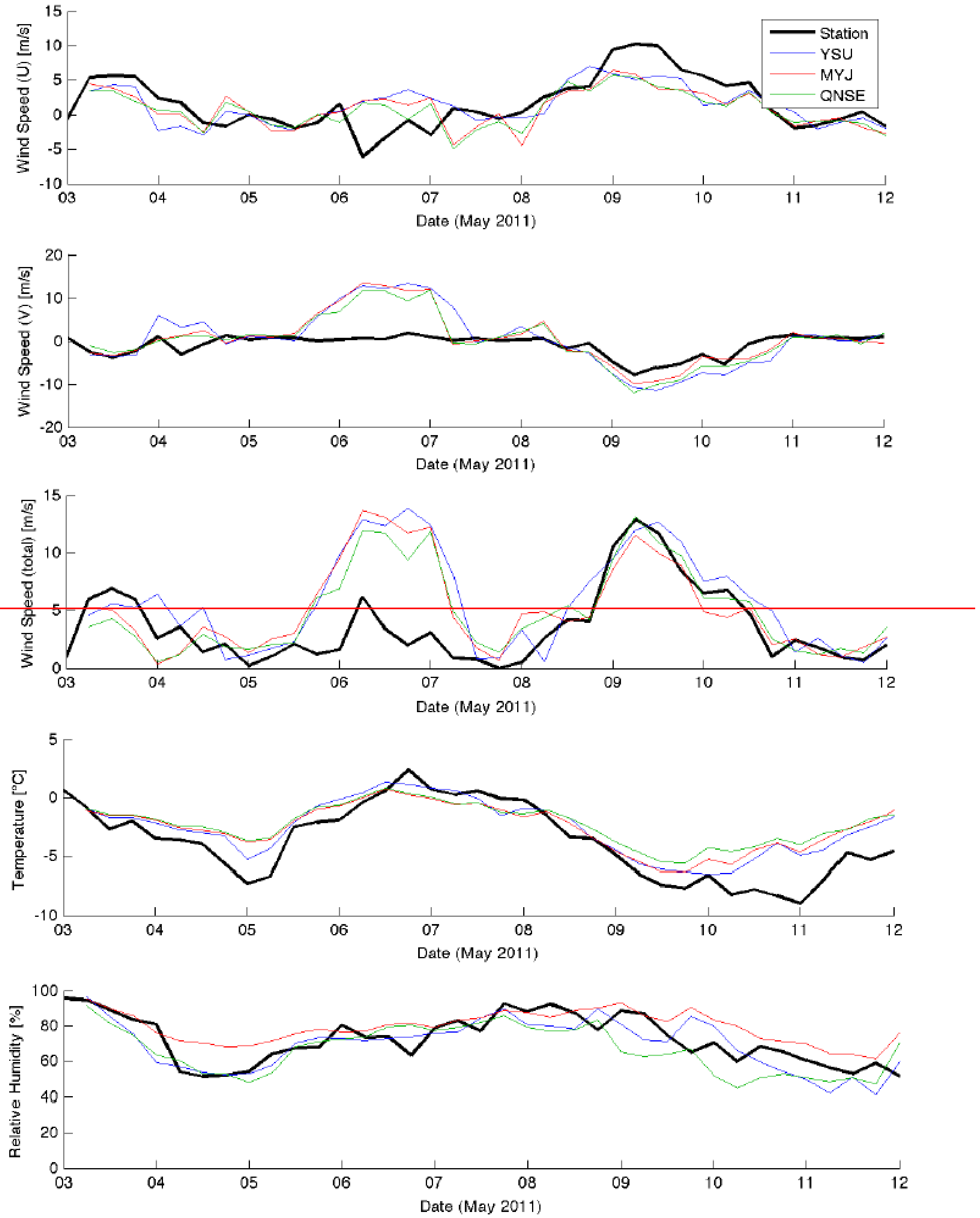
Wind Speed (U) [m/s]
Station
YSU
MYJ
QNSE
Date (May 2011)
Wind Speed (V) [m/s]
Date (May 2011)
Wind Speed (total) [m/s]
Date (May 2011)
Temperature [°C]
Date (May 2011)
Relative Humidity [%]
Date (May 2011)

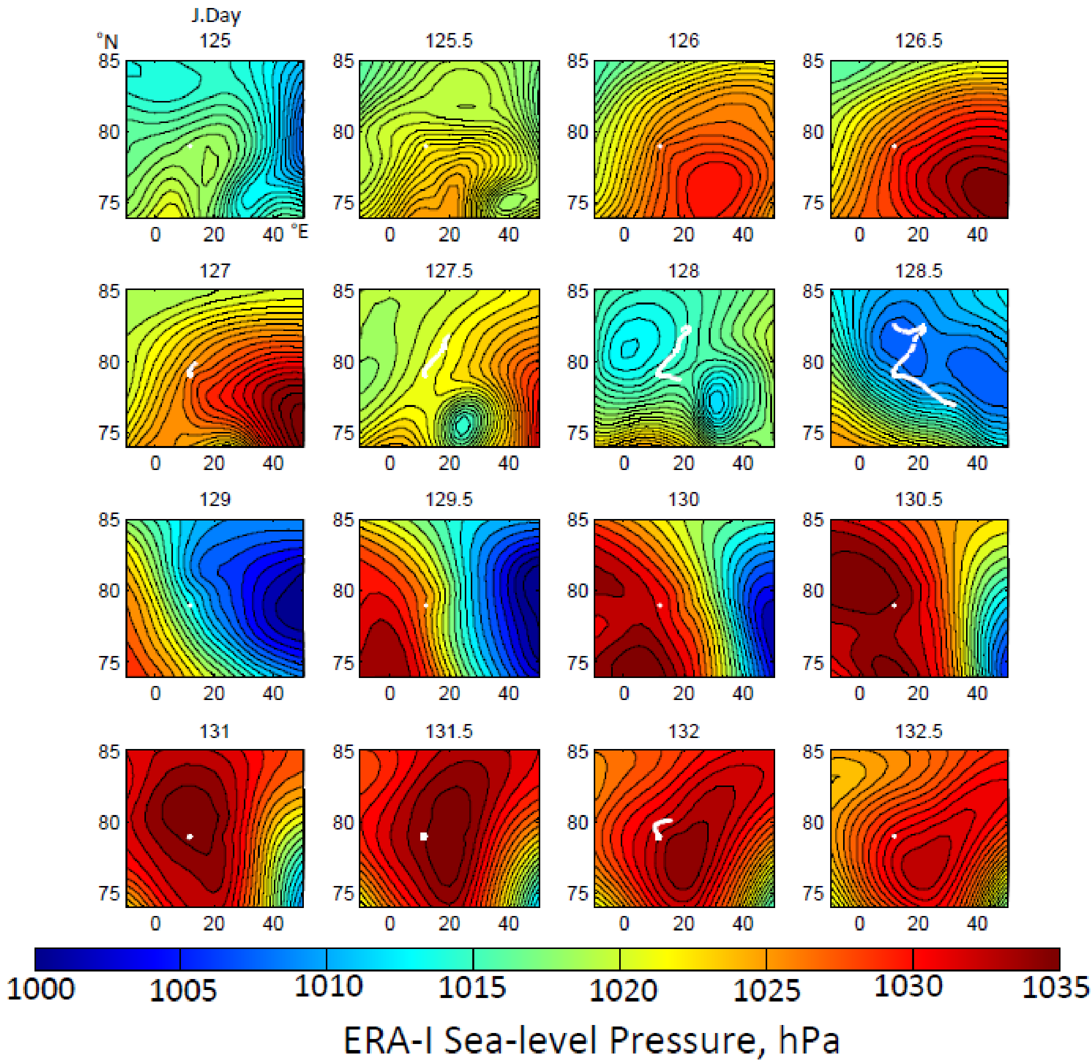

Figure 3. Sea-level pressure in ERA-I shown as a function of latitude and longitude at 12 hrly intervals for the duration of the field-campaign, starting JD 125 (5 May). Overlain in white are Ny-Ålesund location and the CMET flight tracks as a function in time (full extents of flights 3 and 4~~. 6 hourly averaged meteorology~~ are shown at JD 128.5, and for flight 5 at JD 132).

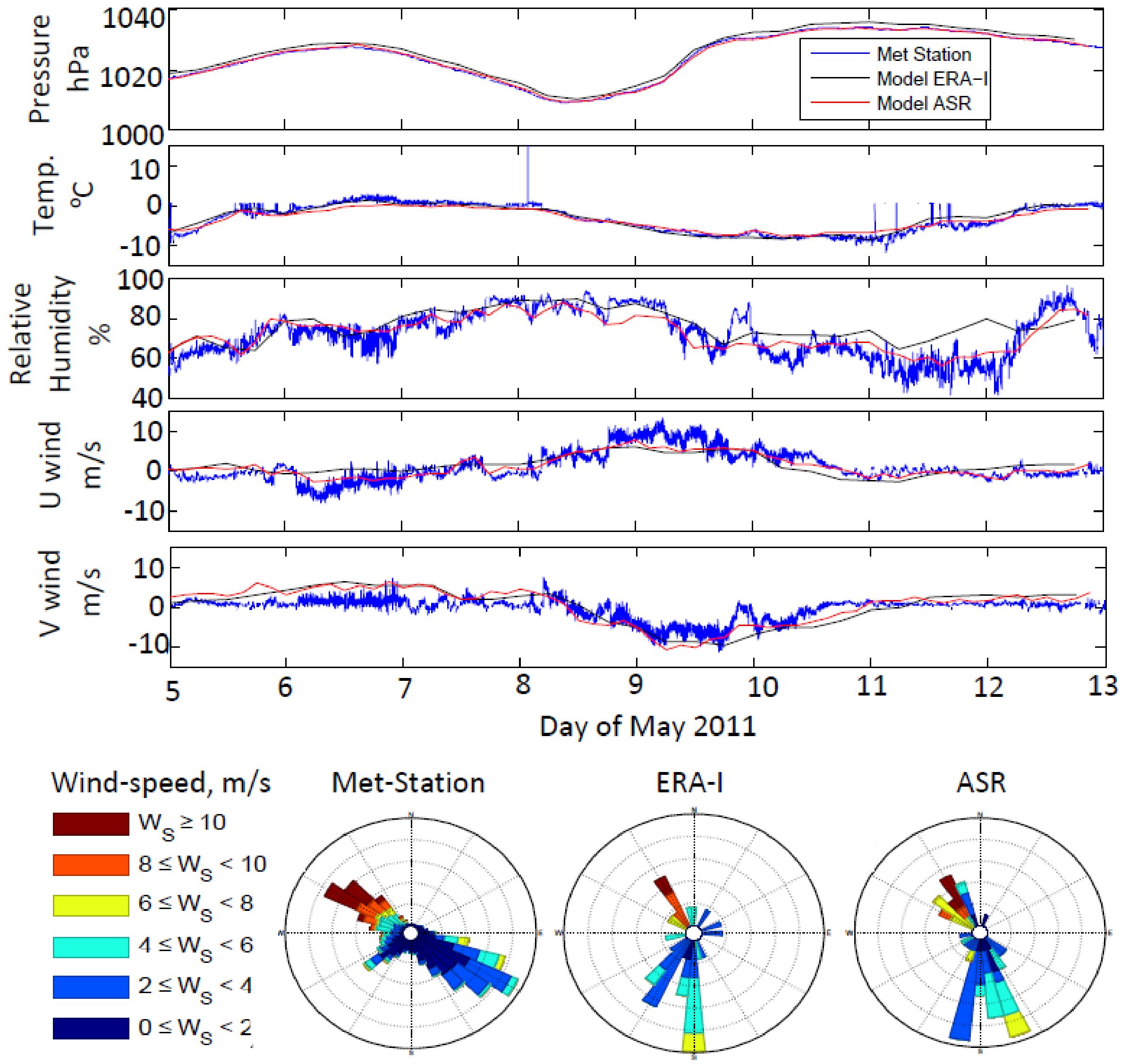

Figure 4

Meteorology parameter time-series (resolution: minutes) from the Ny-Ålesund AWIPEV station compared ~~to WRF~~ERA-I (6 hrly) and ASR (3 hrly) outputs; for pressure, temperature, relative humidity, U and V winds. Wind-roses compare model ~~simulation with 3 boundary layer schemes (YSU, MYJ, QNSE).~~and observed (from) wind directions.

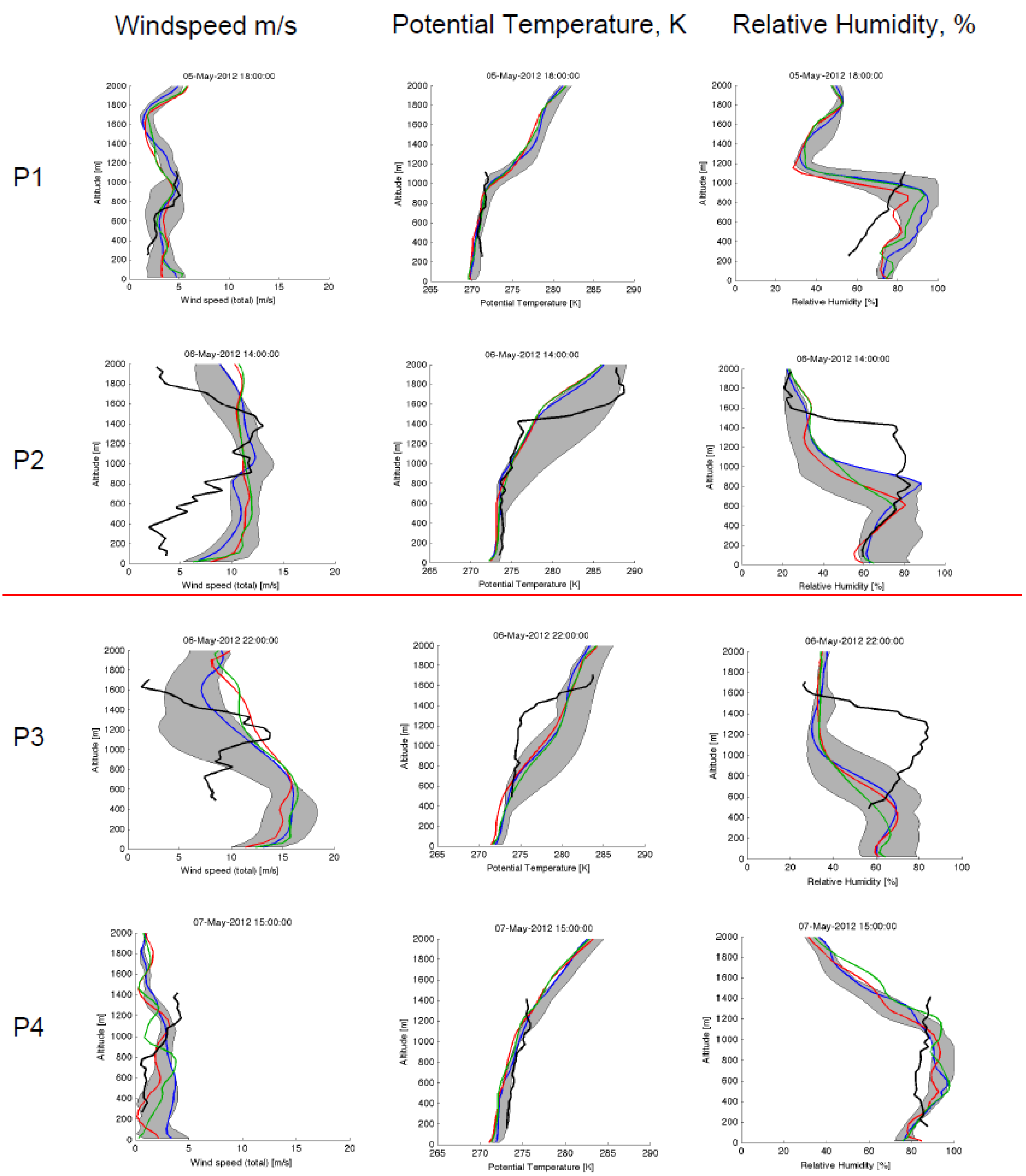

~~Figure 5. CMET wind speed, potential temperature and relative humidity profiles P1-P4 made over Svalbard topography compared to WRF model. The 3 ABL schemes are depicted with the same colour key as for Figure 4. The grey band represents a range of 25 profiles of the YSU scheme on a 4km x 4km square centred the balloon profile to illustrate horizontal variability in the model output.~~

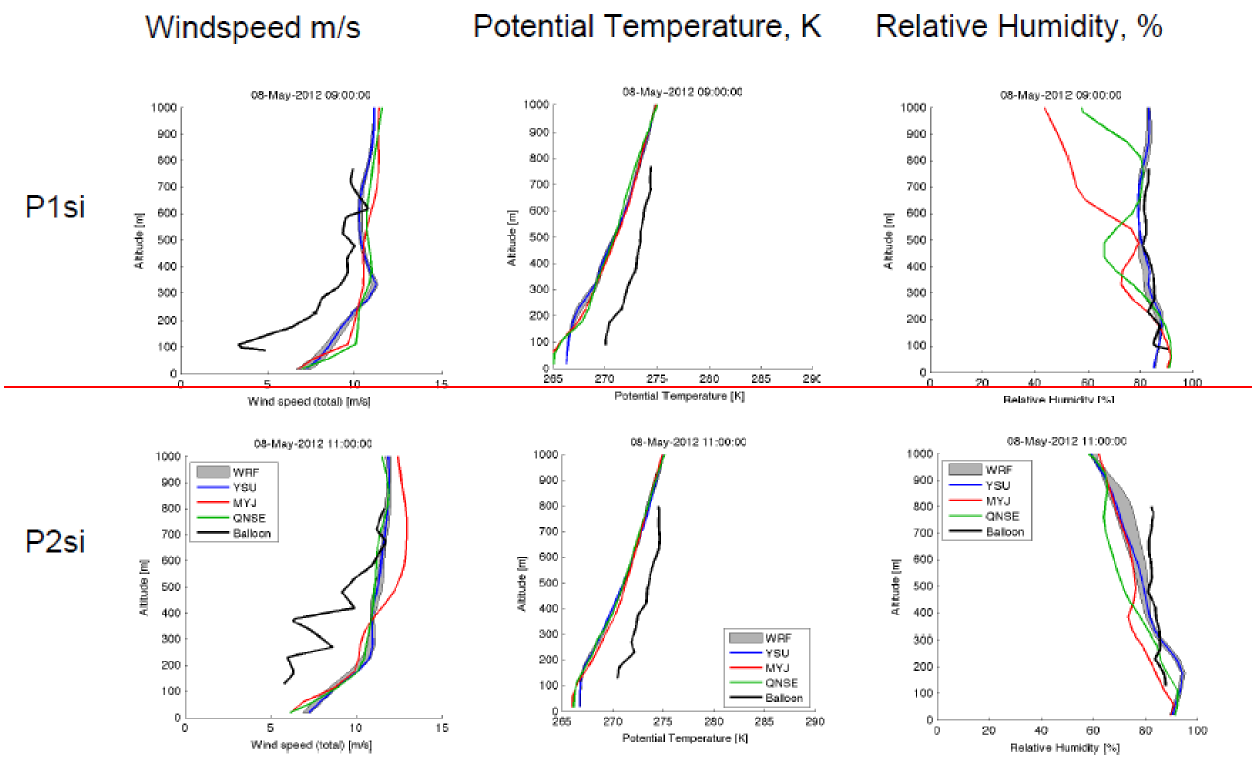

~~Figure 6. As for Figure 5 but for profiles P1si and P2si over sea-ice east of Svalbard.~~

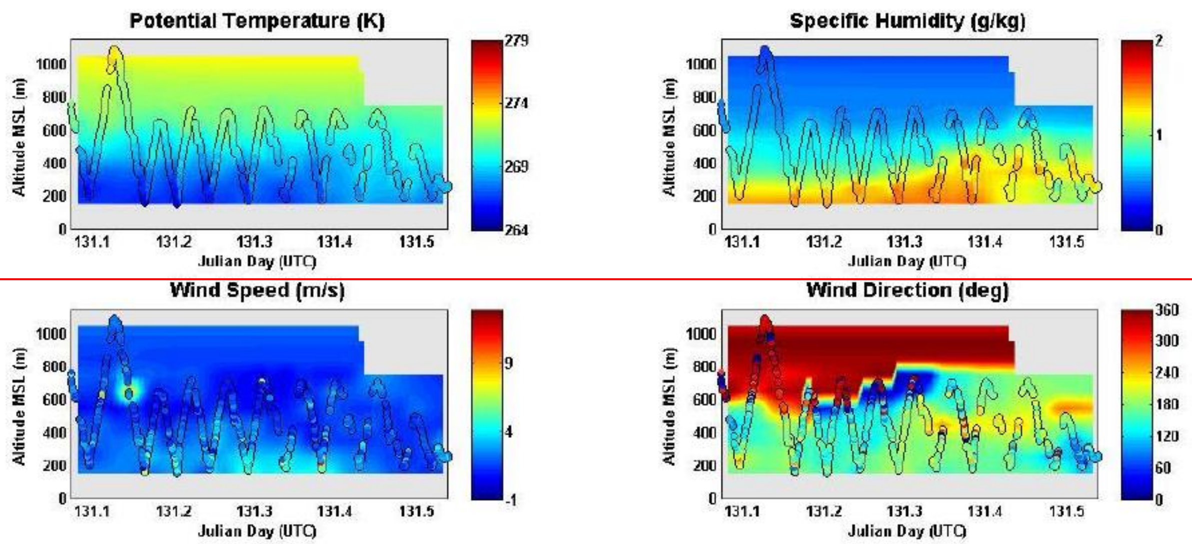
Potential Temperature (K)
Specific Humidity (g/kg)
Wind Speed (m/s)
Wind Direction (deg)
Altitude MSL (m)
Julian Day (UTC)
0
200
400
600
800
1000
131.1
131.2
131.3
131.4
131.5
279
274
269
264
2
1
0
9
4
-1
360
300
240
180
120
60
0

~~Figure~~

~~7.~~

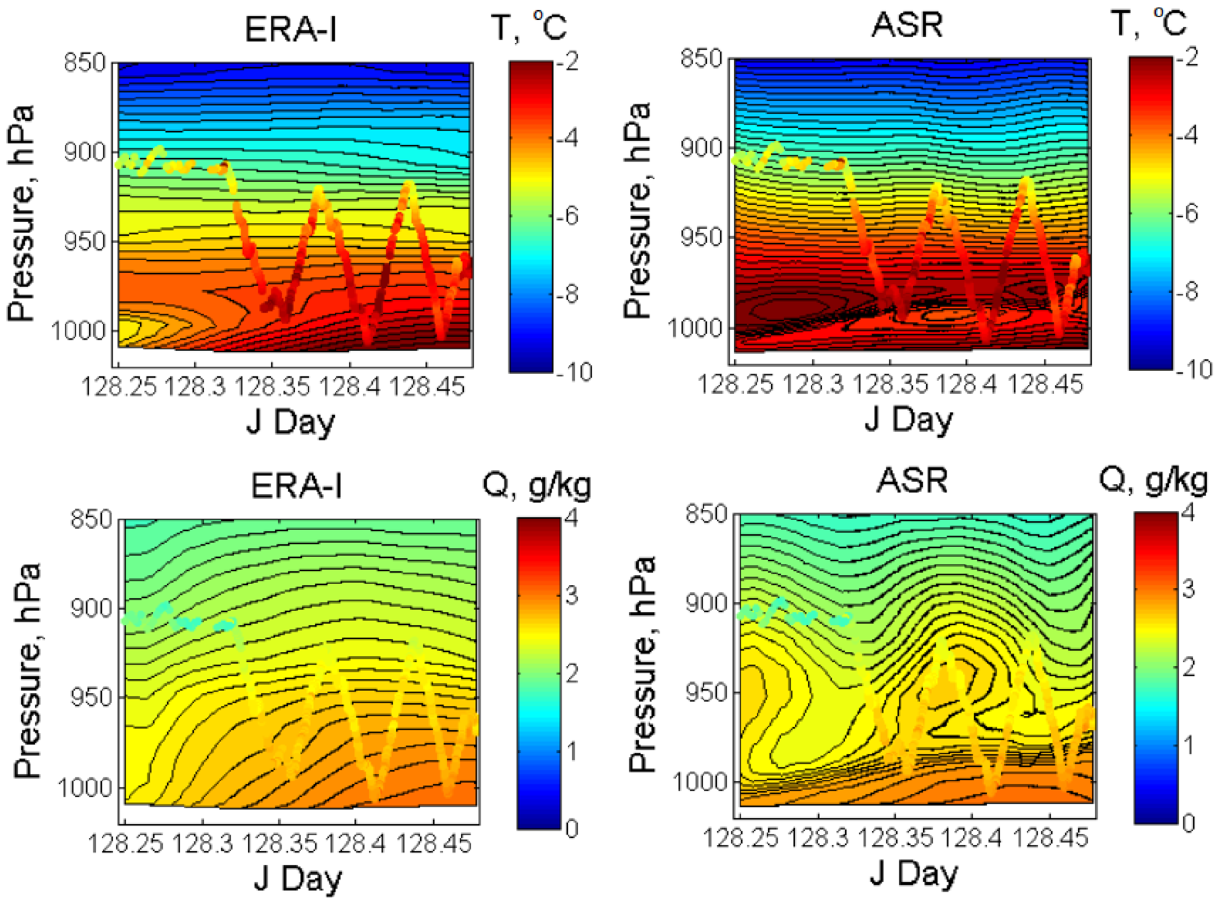
ERA-I
ASR
T, °C
Q, g/kg
Pressure, hPa
J Day
850
900
950
1000
128.25
128.3
128.35
128.4
128.45
-2
-4
-6
-8
-10
4
3
2
1
0

Figure 5. Temperature and specific humidity measured during the CMET flight 4 soundings (filled circles) compared to 4-D interpolated (latitude, longitude, pressure, time) model data from ERA-I and ASR.

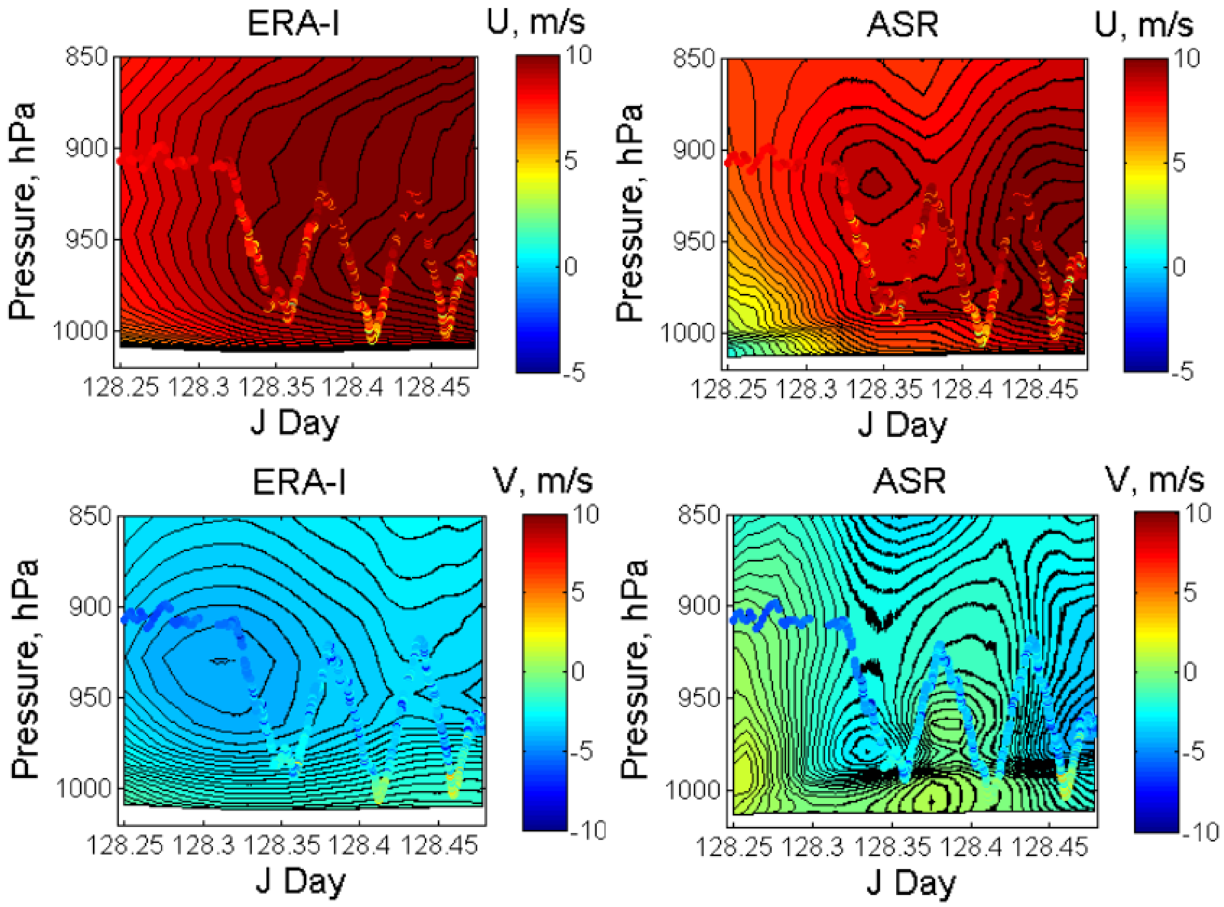

Figure 6. U and V winds observed during the CMET flight 4 soundings (filled circles) compared to 4-D interpolated (latitude, longitude, pressure, time) model data from ERA-I and ASR.

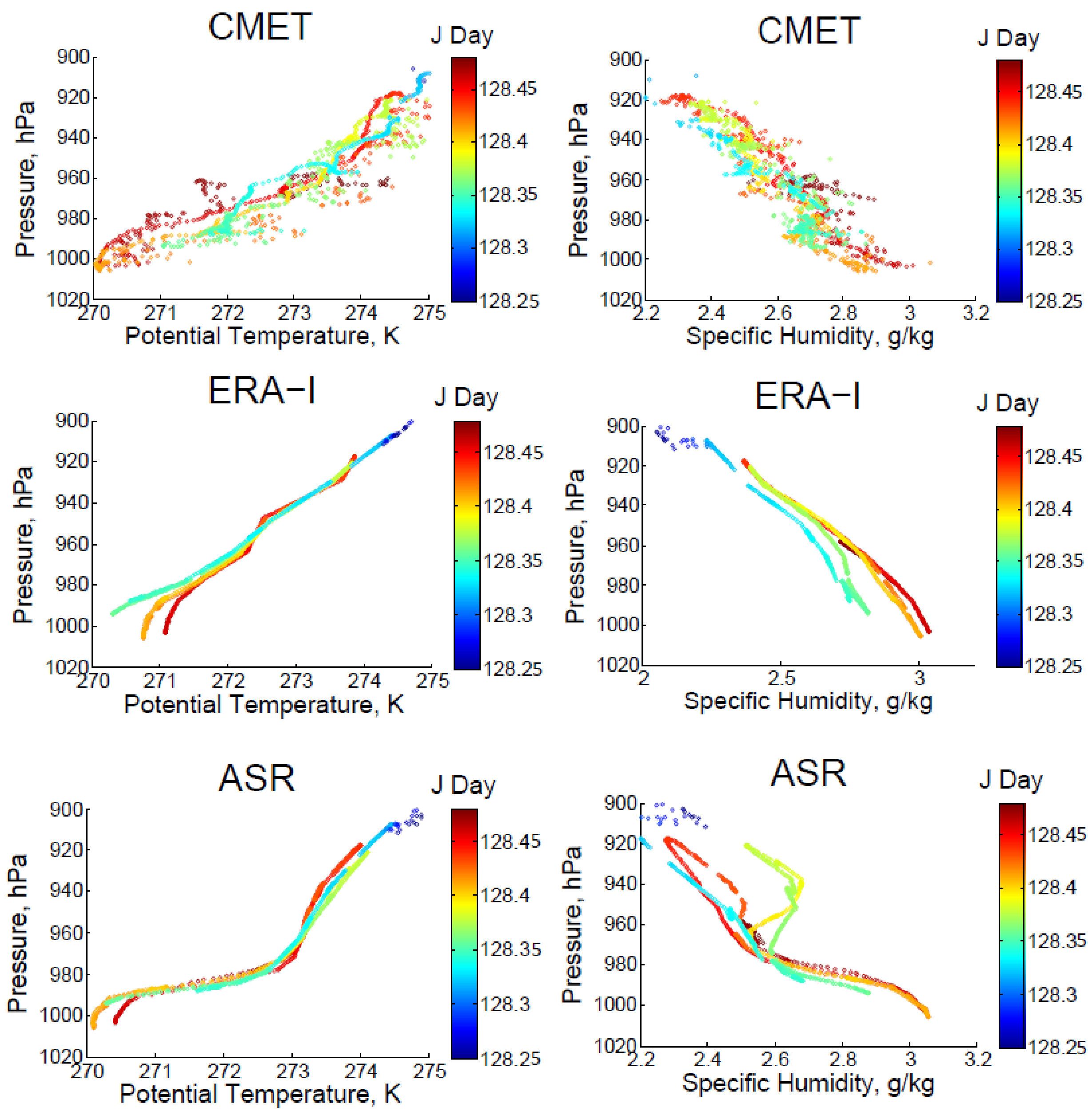

Figure 7. Profiles of potential temperature and specific humidity during flight 4 as observed by the CMET balloon and according to the 4-D interpolated ERA-I and ASR model outputs.

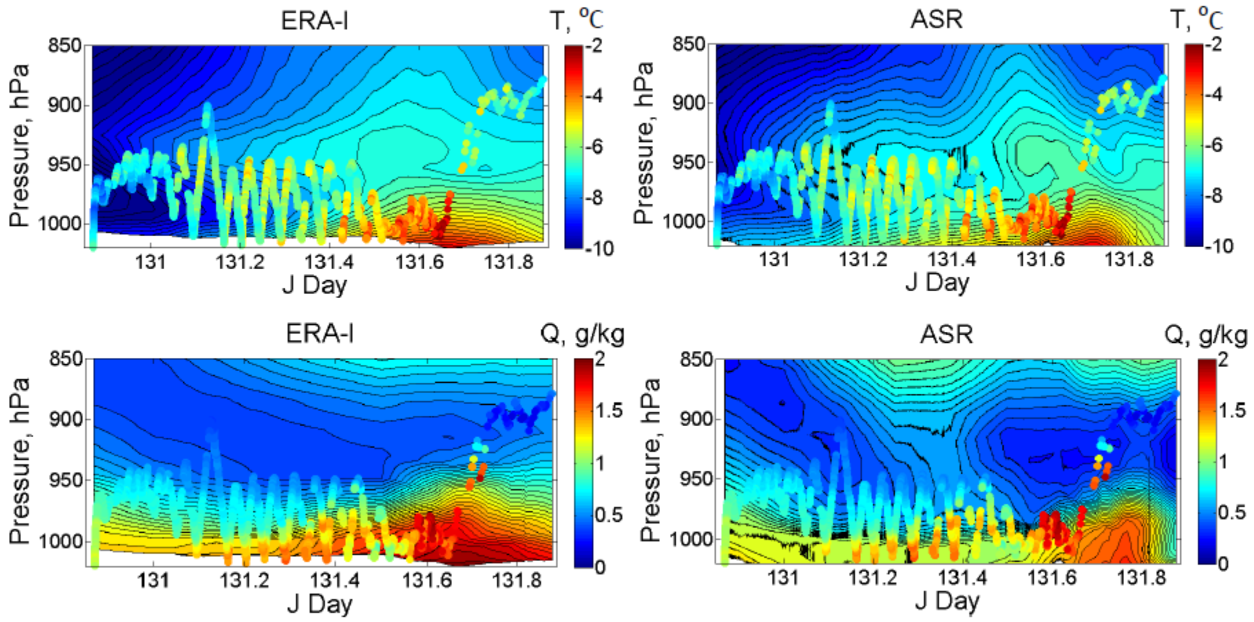

Figure 8. Temperature and specific humidity measured during the CMET flight 5 soundings (filled circles) compared to 4-D interpolated (latitude, longitude, pressure, time) model data from ERA-I and ASR.

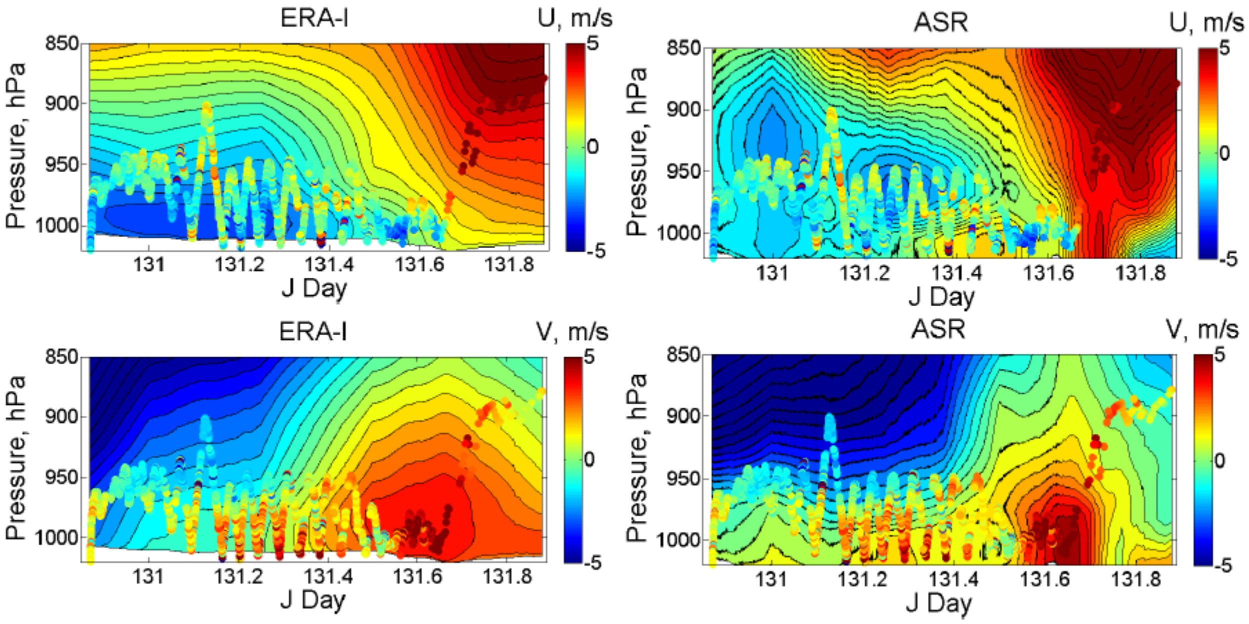

Figure 9. U and V winds observed during the CMET flight 5 soundings (filled circles) compared to 4-D interpolated (latitude, longitude, pressure, time) model data from ERA-I and ASR.

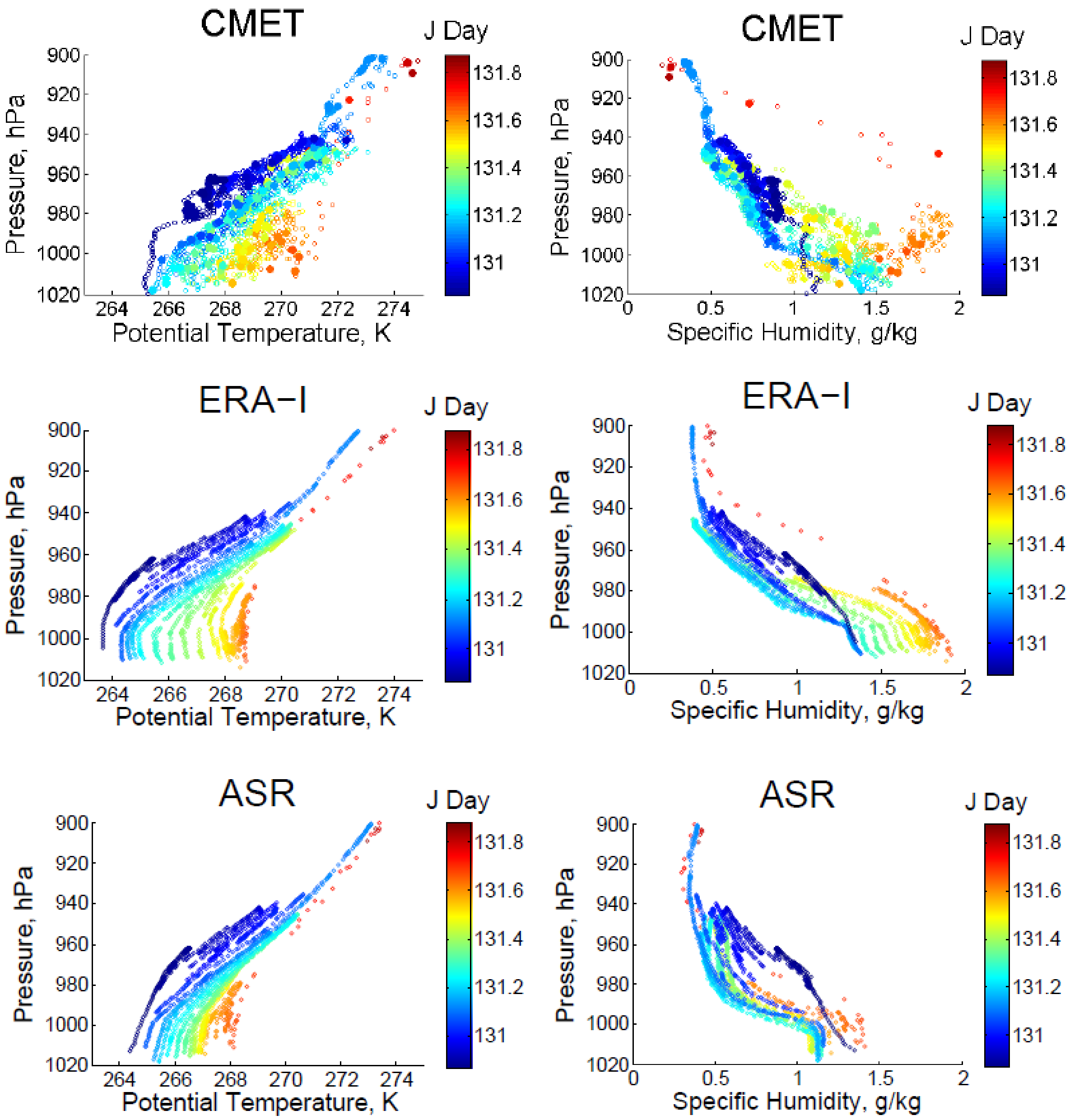

Figure 10. Profiles of potential temperature and specific humidity during flight 5 as observed by the CMET balloon and according to the 4-D interpolated ERA-I and ASR model outputs. CMET measurements made during descents only (> 0.1 m/s vertical descent speed) are shown as filled circles with full data-set shown as open circles.

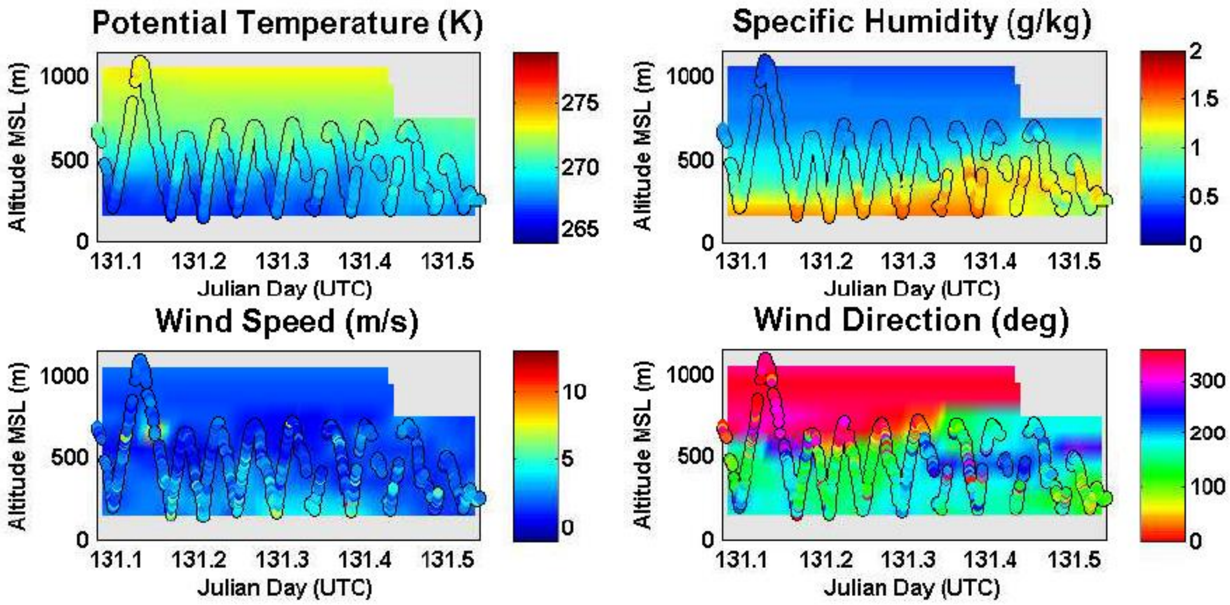

Figure 11. Potential temperature, specific humidity, wind-speed and wind direction determined from the CMET balloon observations (131.08 to 131.52 JD, equivalent to ~~~2~~02 to 12.5 UTC on 11 May) of flight 5 during a series of automated soundings between 150 m and 700 m altitude. Data between the balloon soundings has been interpolated ~~to facilitate visualization~~.

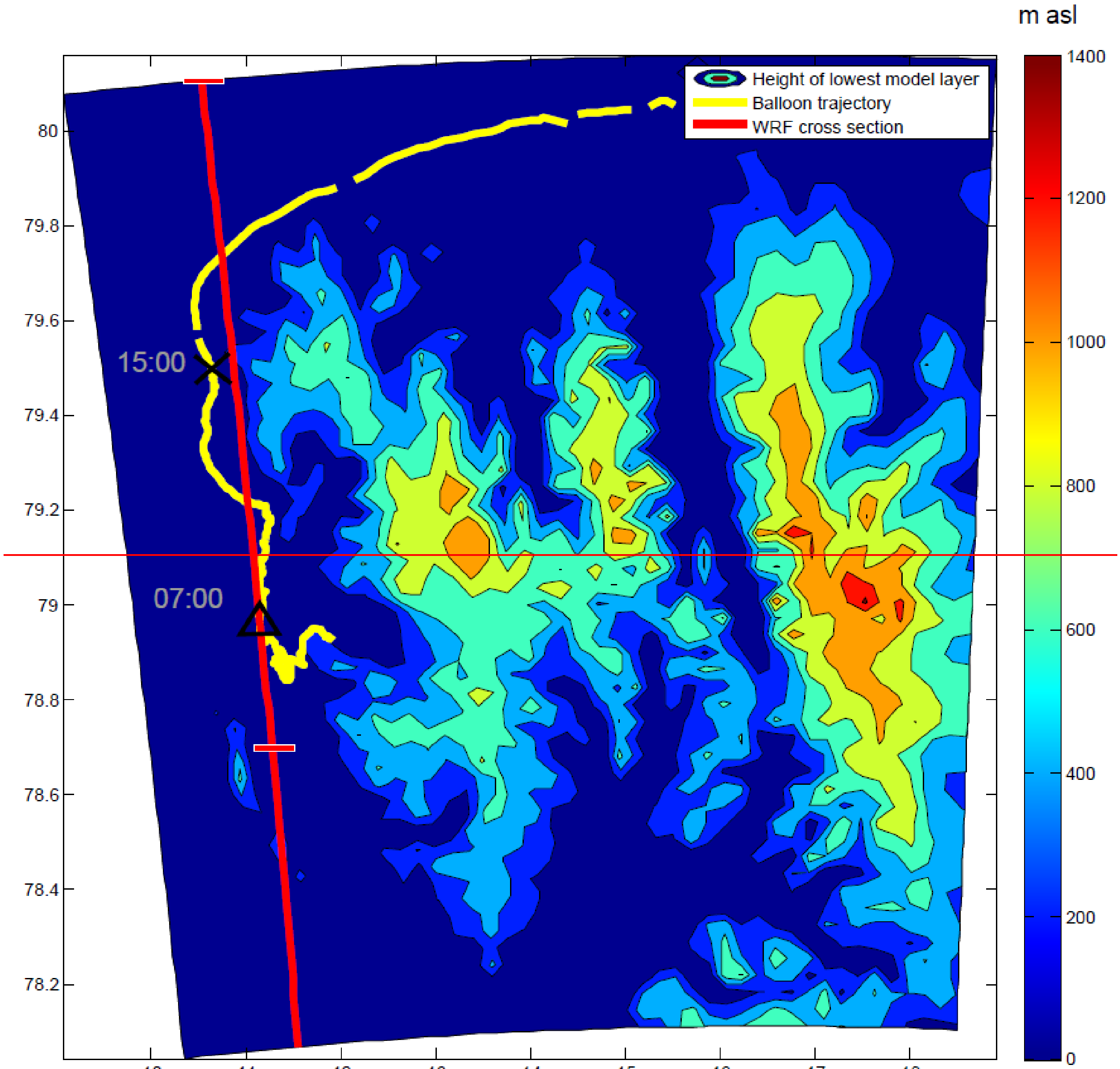
m asl
Height of lowest model layer
Balloon trajectory
WRF cross section
15:00
07:00
80
79.8
79.6
79.4
79.2
79
78.8
78.6
78.4
78.2
10
11
12
13
14
15
16
17
18
1400
1200
1000
800
600
400
200
0

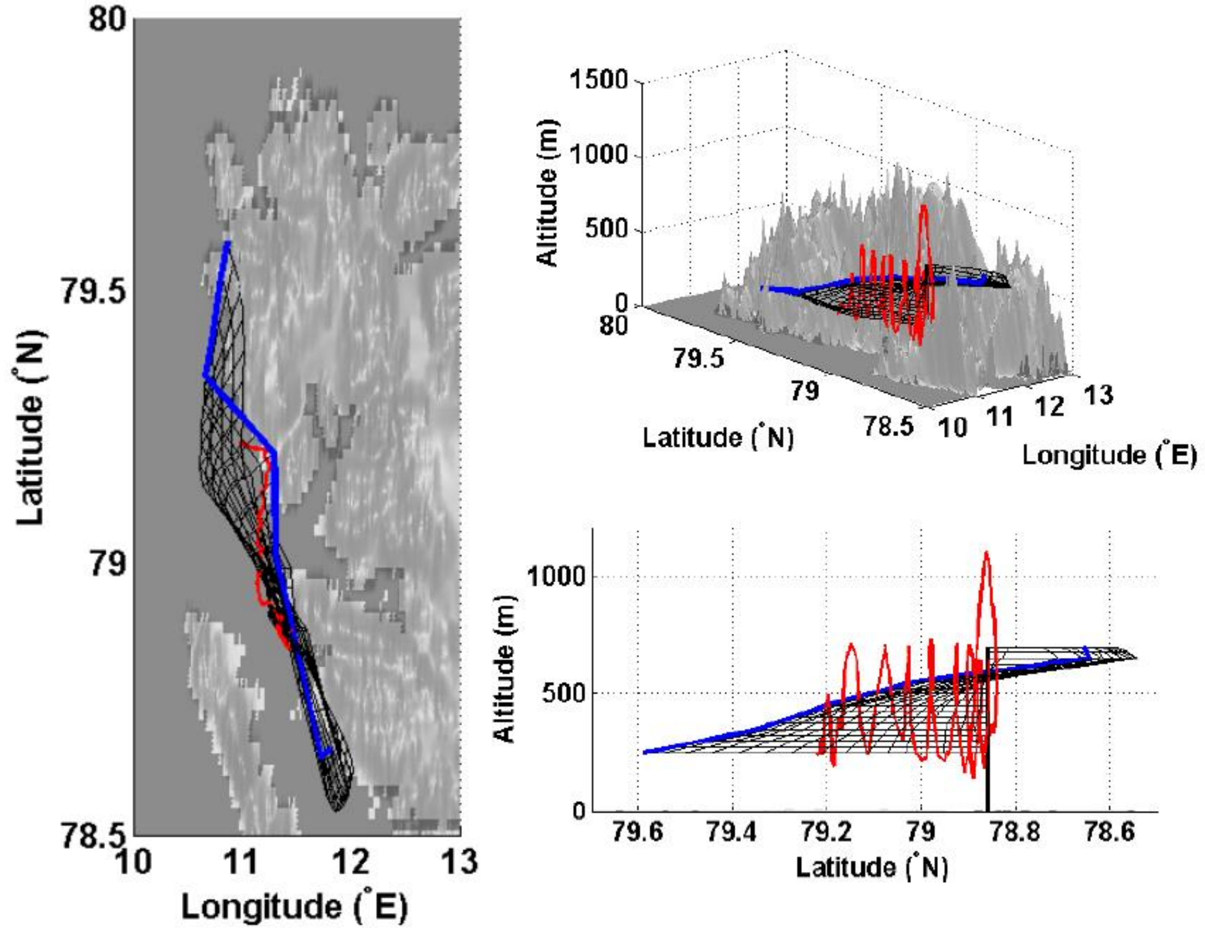

~~Figure 8. Map of the WRF cross-section transect (red lines) and the CMET balloon trajectory (yellow line) of flight 5. Approximate balloon locations at 07h and 15h UTC (JD 131.3 and 131.6) are denoted by a triangle and cross, respectively.~~

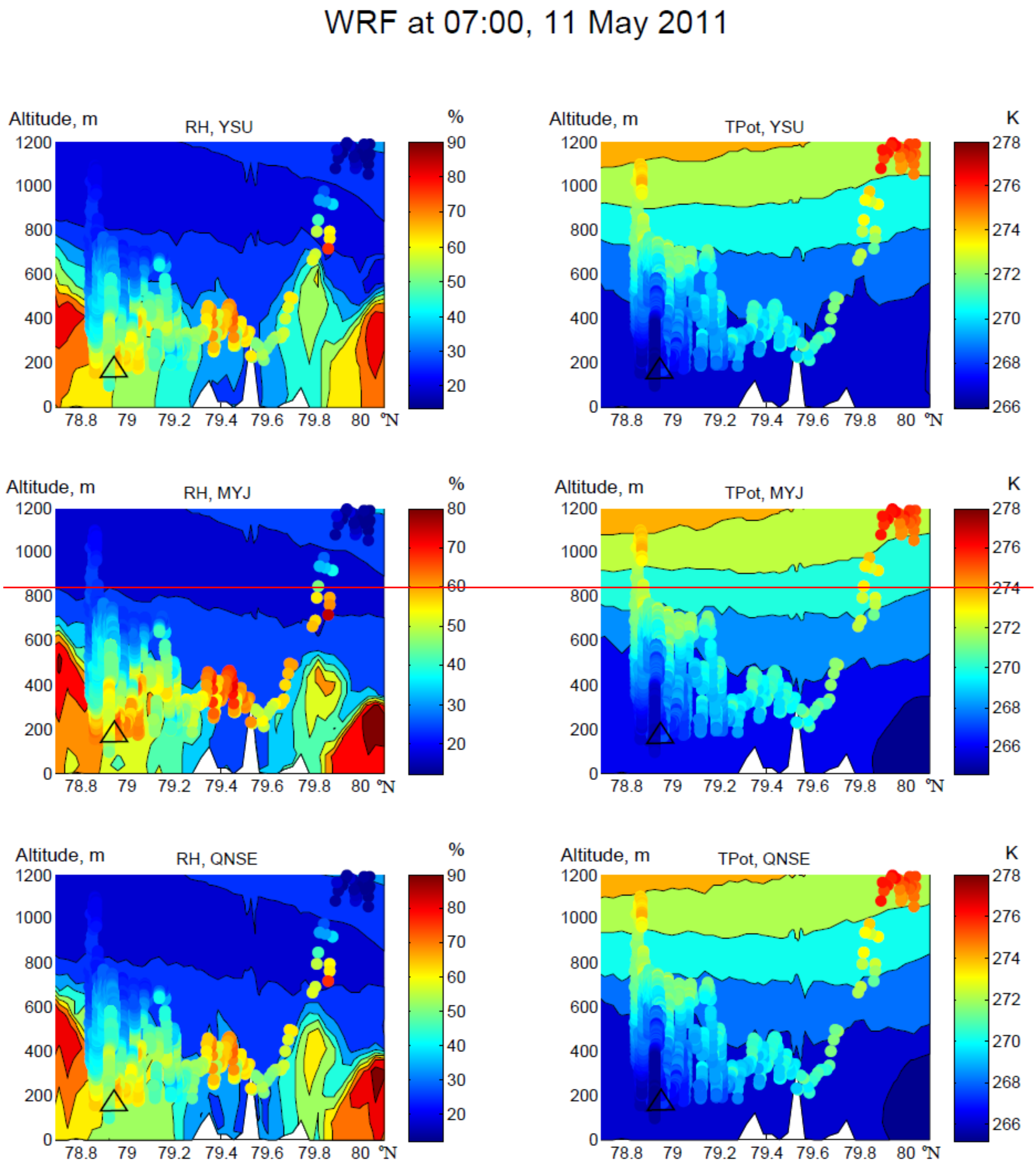

~~Figure 9. Crossection of the WRF model relative humidity (RH) and potential temperature (TPot) at 07h UTC (JD 131.3) shown as a function of altitude along the transect line. CMET observations for the whole flight are also illustrated, with approximate balloon location at 07h denoted by a triangle.~~

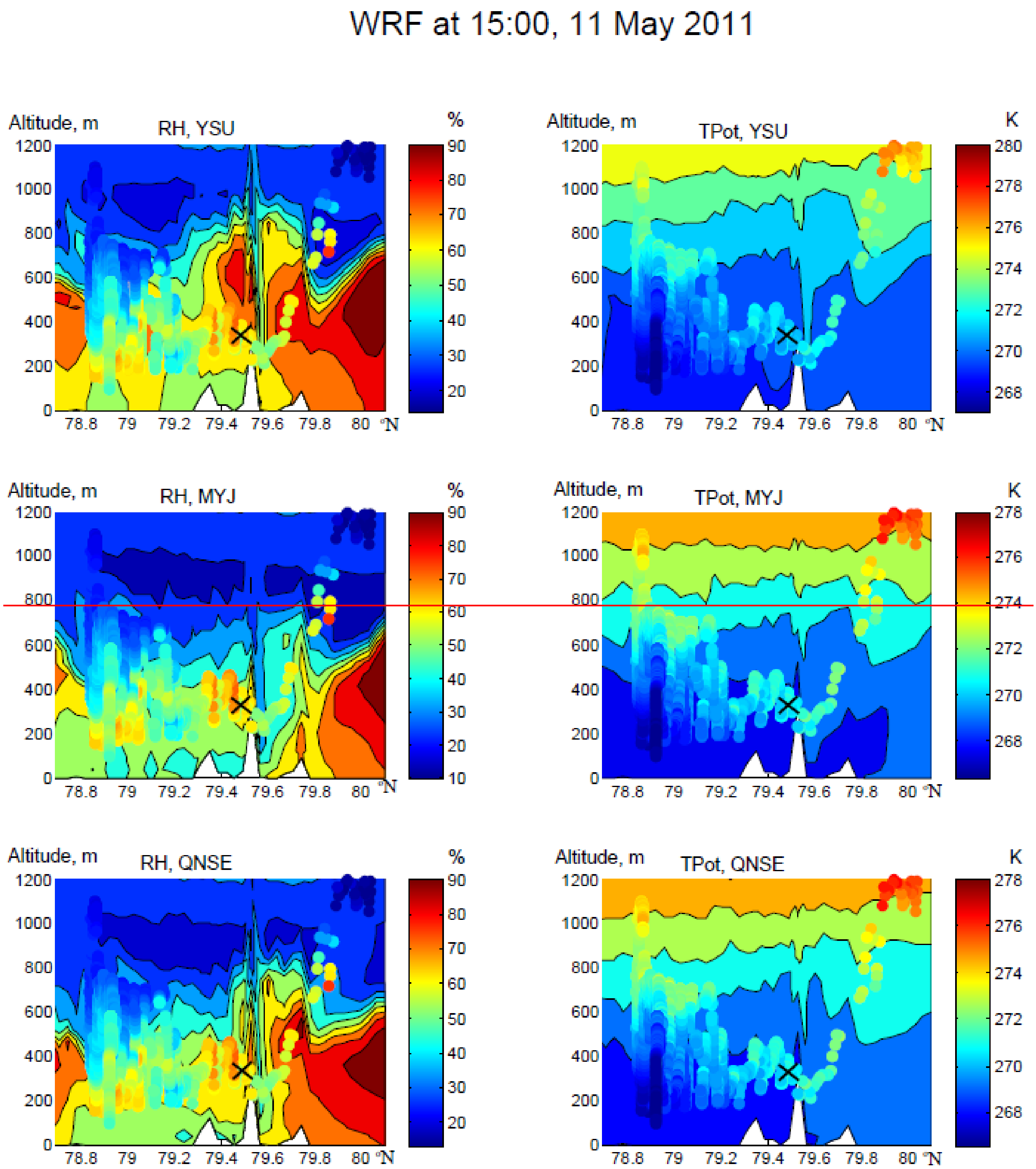

~~Figure 10. Crossection of the WRF model relative humidity (RH) and potential temperature (TPot) at 15h UTC (JD 131.6) shown as a function of altitude along the transect line. CMET observations for the whole flight are also illustrated, with approximate balloon location at 15h denoted by a cross.~~

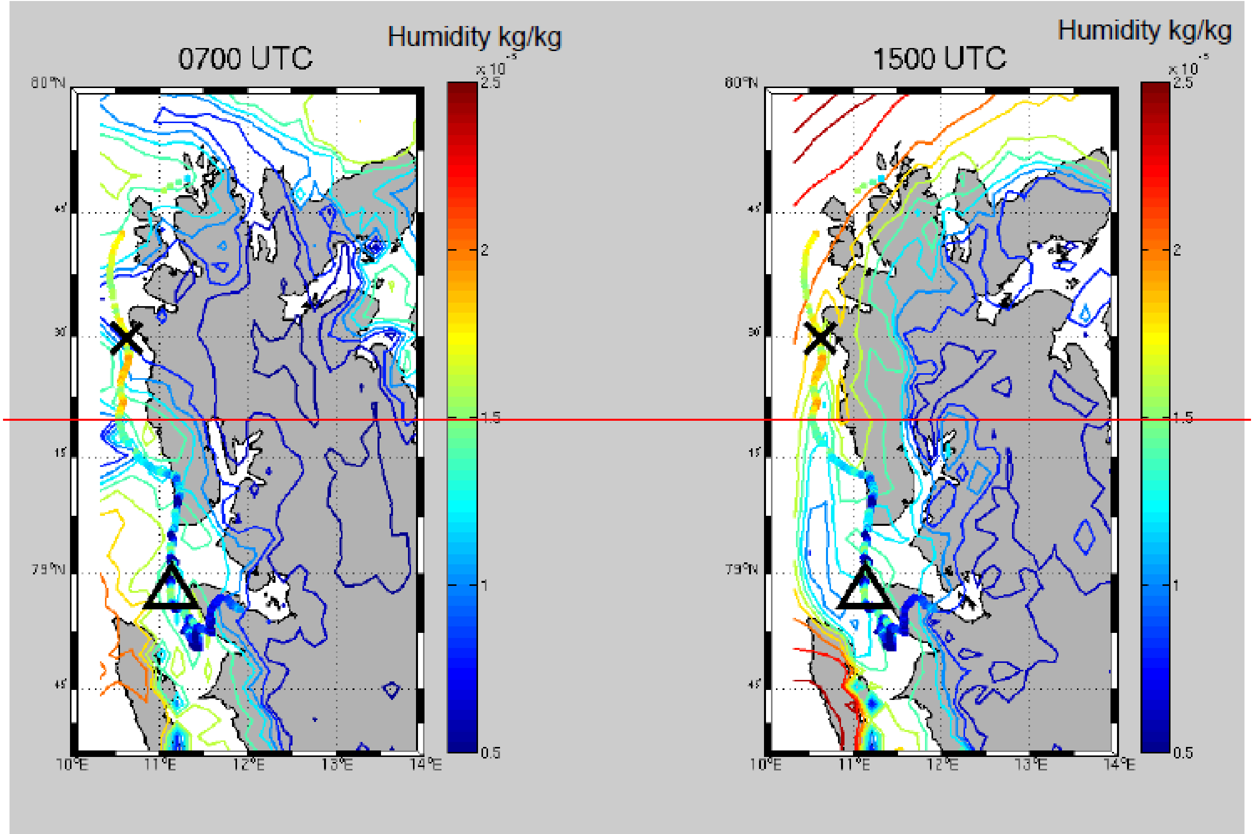

~~Figure 11. Absolute humidity (kg/kg) in the WRF model (with MYJ scheme) layer corresponding to 300 masl (over oceans) at 07h and 15h compared to the CMET flight 5 whilst it performed automated ABL soundings centred around ~300 masl. The CMET balloon positions at 07h and 15h (equivalent to JD 131.3 and JD 131.6) are marked by a triangle and a cross, respectively. Data from the final stages of the balloon flight (at greater than ~1000 m asl thus not probing the ABL) has been omitted for clarity.~~

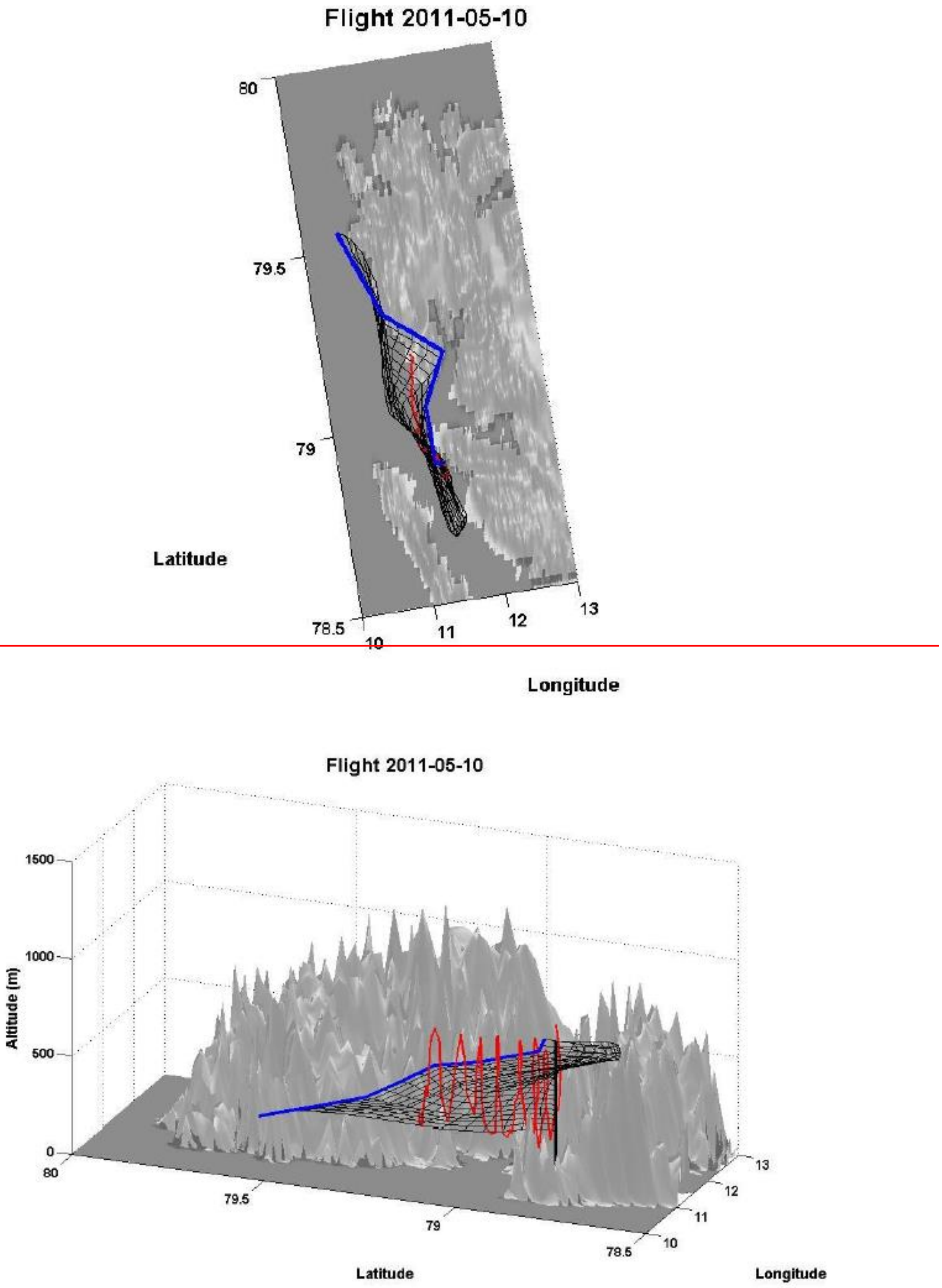

Figure 12.~~Approximate air-parcel trajectories~~ Wind-field calculated from the CMET balloon~~-measured winds. The~~ flight 5. Air parcel trajectories are calculated over an eight hour period for each 50 m altitude layer~~.~~ according to the winds observed by the CMET soundings. The red line shows the actual balloon track, the black vertical line shows the initialization~~, the black~~ of the calculation, and the derived air parcel trajectories (wind field grid~~ shows the trajectories, and~~) are shown in gray. The blue line shows the final ~~location~~locations after eight hours.

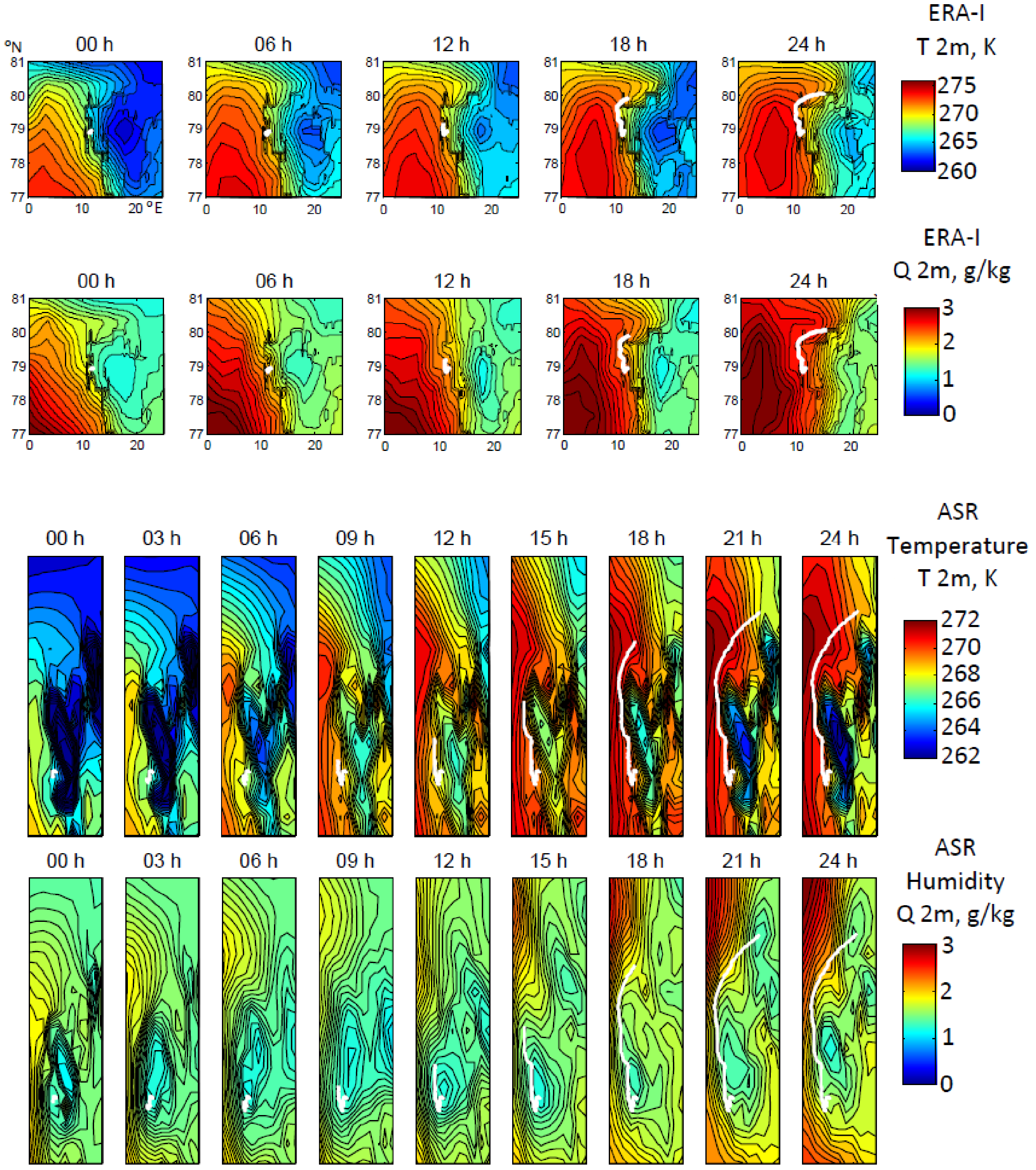

Figure 13. Surface 2m temperature and specific humidity over JD 131 according to ERA-I (upper) and ASR (lower). ERA-I outputs shown on the regional scale at 6 hrly intervals whilst ASR outputs are shown on a local scale at 3 hrly intervals. The CMET flight 5 trajectory up to each time-point is illustrated shown as a white line.

1